



A novel method for the remediation of wastewater containing acid red 131 dye using acoustic cavitation combined with sulphur-doped TiO₂ and oxidants

Subhamita Das · Chandrodai Agarkoti ·
Parag R. Gogate

Received: 9 January 2023 / Accepted: 3 July 2023 / Published online: 20 July 2023
© The Author(s), under exclusive licence to Springer Nature Switzerland AG 2023

Abstract The present study investigated the degradation of Acid Red 131 (AR131) dye using a combination of ultrasound-induced cavitation, ultraviolet (UV) irradiation, chemical oxidants, and photocatalyst, focusing on the effect of operating parameters. It was established that acidic pH, higher input power, and lower initial concentration resulted in higher degradation. Sulphur-doped titanium dioxide (S-TiO₂) synthesized using a novel ultrasound-assisted method showed an optimum dosage of 300 ppm for the AR131 degradation with sulphur to titanium ratio of 2:1. In the combination approach, the optimum dosage of hydrogen peroxide (H₂O₂) and potassium persulfate (KPS) was established as 100 ppm and 400 ppm respectively. The maximum degradation of 90.3% was obtained using a combined approach of US+KPS+UV/S-TiO₂ whereas, a maximum synergetic coefficient of 1.57 was obtained for the approach of US+UV/S-TiO₂ with degradation of 86.96%. It was also elucidated that for combination approaches of US+H₂O₂, US+H₂O₂+KPS, and US+H₂O₂+KPS+UV/S-TiO₂, the synergetic coefficients were lower than one due to undesirable side reactions and radical scavenging. Scale-up studies performed at 15 times of the laboratory scale volume, elucidated that the maximum degradation was obtained as 58.01% for the approach

of US+KPS+UV/S-TiO₂. Therefore, the approach of US+KPS+UV/S-TiO₂ was elucidated as the most efficient in degrading the AR131 dye at both small and large scale of operation. In terms of synergy, the approach of US+UV/S-TiO₂ was more efficient. Overall, an optimized combination approach was successfully demonstrated for the effective degradation of AR131 dye with synergism and better results at a large scale.

Keywords Advanced oxidation processes · Sonochemistry · Ultrasonic reactor · Photocatalyst synthesis · Sulphur doped titanium dioxide

Introduction

The textile industry significantly contributes to industrial production worldwide, although it also has an immense environmental impact. Effluent from the textile industry contains an enormous variety of synthetic dyes in higher concentrations (Reza et al., 2017), which offers significant environmental concerns due to its high toxicity and long half-lives coupled with hazardous nature of dyes. When released into the environment, the dyestuff molecules can contaminate the nearby soil, sediment, and surface water and disrupt the ecosystem (Zafar et al., 2021). These molecules also prevent aquatic plants or algae's biological activities (photosynthesis) and can accumulate in the fishes showing

S. Das · C. Agarkoti · P. R. Gogate (✉)
Department of Chemical Engineering, Institute
of Chemical Technology, Matunga, Mumbai 40019, India
e-mail: pr.gogate@ictmumbai.edu.in

cytotoxic effects. The presence of dyes also alters the natural pH of the water and increases the chemical oxygen demand (COD) as well as the biochemical oxygen demand (BOD) (Slama et al., 2021). Sometimes, due to a half-life of several years, their quantitative presence in the environment is quite significant. The most commonly applied synthetic dyes are the azo dyes (Yaseen & Scholz, 2019) which have applications in the leather processing and textile industry. The azo dyes are cheaper, easier to use, and provide strong colours. On the other hand, they are also toxic, mutagenic, and carcinogenic when present above a certain concentration in wastewater (Batra et al., 2022). Under certain conditions, cleavage of the $-N=N-$ azo bond occurs to form the $-NH_2$ (Amino) group, which has the potential to cause cancer (Kongor et al., 2021). Thus, completely removing the azo dyes is of utmost importance in wastewater treatment plants and hence, it is essential to develop effective methods of treatment that elucidate the importance of current work.

Acid Red 131 (AR131) dye belongs to the mono-azo dye group, which is extensively used for dyeing polyamide fibres, nylon, wool, and silk in the textile industries. The molecular structure of the dye is shown in Fig. 1. AR131 is primarily a sodium salt of sulfonic and carboxylic acids and is known to cause aesthetic pollution along with toxicity (Khandegar & Saroha, 2014). The limited information about this dye and its susceptibility to different oxidation approaches makes it an interesting topic for research.

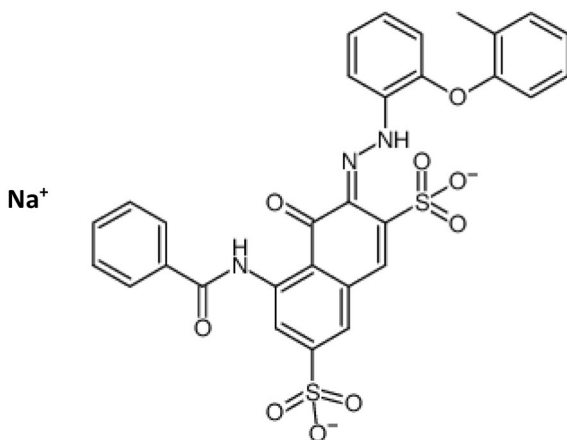


Fig. 1 Molecular structure of Acid Red 131 dye

Generally, biological oxidation is the applied method for wastewater treatment, and researchers have shown that decolorization of azo and diazo dyes is possible using different microbial cultures (Kamal et al., 2022), though a significant amount of time is required. Bera and Tank (2021) reported complete degradation of Procion Red—H3B using *Pseudomonas stutzeri*, however, almost 20 h were required for the degradation. Similarly, Rajashekharappa et al. (2022) reported almost complete decolourization of both Fat Red E and Amarnath RI at initial loading of 5 mg/L using *Geobacillus thermoleovorans* KNG 112 within five days. In addition to biological oxidation, some studies have been targeted based on electrochemical oxidation. Wijetunga et al. (2012) used anaerobic consortia for the degradation of Acid Red 131 and reported that 81% degradation was obtained after 45 h of treatment. (Khandegar & Saroha, 2014) treated the synthetic solution consisting of Acid Red 131 dye and obtained a colour removal efficiency of 98% within 180 min using the electrochemical treatment method. Similarly, Nayebi et al. (2021) reported the maximum removal extent of Acid Red 131 as 98% within 180 min using the electrochemical process. Considering the extensive time required for biological oxidation and only a limited study dealing with AR131 degradation, that too based on electrochemical methods, alternative advanced oxidation processes (AOPs) has been targeted in the present work, clearly establishing the novelty of the work. The AOPs are based on the attack of $\bullet OH$ radicals on recalcitrant organic pollutants, leading to degradation at significant rates. Though effective in mineralization, AOPs require oxidants that can be expensive compared to biological processes (Almomani et al., 2016; Ghumra et al., 2021). Therefore, an advanced combination technique such as cavitation in combination with the AOPs can be applied to reduce the quantity of the oxidants and the degradation time (Gogate, 2022). The present study focuses on using acoustic cavitation combined with AOPs for the degradation of AR131 dye.

Heterogeneous photocatalysts such as TiO_2 have been generally applied for contaminant degradation, including various dyes based on the generation of $\bullet OH$ radicals, due to the series of reactions occurring when the photocatalyst is excited by the absorption of the incident light, mainly UV irradiations. The catalyst typically remains unchanged after the degradation process, and negligible sludge is generated, which does not need disposal (Ibhadon & Fitzpatrick, 2013). TiO_2 is a highly functional, non-toxic, and long-term stable

photocatalyst that is active only under UV irradiation due to its large band gap energy (Karpuraranjith et al., 2022). The optimization of the spectral properties of TiO_2 has been reported by its doping with non-metal elements such as sulphur (S), nitrogen (N), and fluorine (F) (Akhter et al., 2022). The doping alters the band gap energy and red-shifts the excitation wavelength to the visible region, offering cost-effective operation (Prabakaran & Pillay, 2019). The ionic radius of S is typically larger compared to N and F. Hence, introducing S at the O sites is more efficient as it considerably modifies the electronic structure of TiO_2 (Akhter et al., 2022). Therefore, in the present study, the combination of S- TiO_2 along with cavitation and oxidants has been elucidated for the maximum degradation of AR131 dye, also focusing on the synthesis of S- TiO_2 .

In the present study, the AR131 dye was successfully degraded using US horn at a small scale, and US reactor at a large scale, combined with various oxidants and heterogeneous catalysts as sulphur-doped titanium dioxide (S- TiO_2). The S- TiO_2 was successfully synthesized and characterized to affirm the effective doping of the sulphur into the TiO_2 photocatalyst. The influential parameters such as pH, input power, and initial concentration were initially optimized for enhancing of the extent of AR131 degradation using individual methods and then applied in a combination approach to study synergism. As per our literature survey, the synergistic effect of the US-induced cavitation and S- TiO_2 has not been reported previously. Hence, the study is very important in showcasing the efficacy of combined oxidation approaches at small and large scales.

Materials and methods

Materials

Acid red 131 (molecular weight: 654.622 g/mol, and molecular formula: $\text{C}_{30}\text{H}_{21}\text{N}_3\text{NaO}_9\text{S}_2^-$) was used as the target pollutant. The dye was obtained from the dye house existing in the Department of Fibres and Textile Processing Technology, Institute of Chemical Technology, Mumbai. Titanium isopropoxide ($\text{C}_{12}\text{H}_{28}\text{O}_4\text{Ti}$) and ethanol ($\text{C}_2\text{H}_5\text{OH}$) were procured from Sigma Aldrich. Acetone ($\text{C}_3\text{H}_6\text{O}$), methanol (CH_3OH), sodium hydroxide (NaOH), thiourea ($\text{CH}_4\text{N}_2\text{S}$), hydrogen peroxide (H_2O_2), and potassium

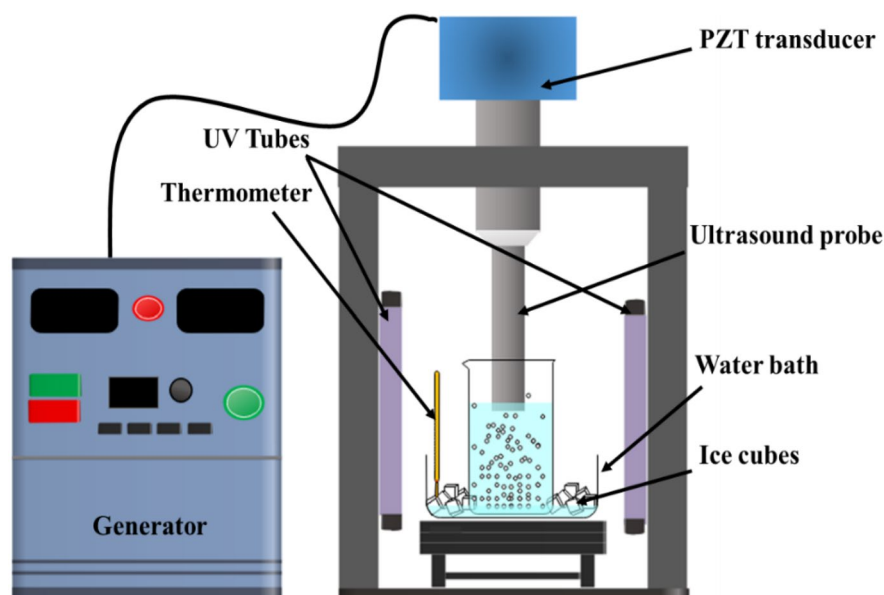
persulfate ($\text{K}_2\text{S}_2\text{O}_8$) were obtained from Molychem. All chemicals were of analytical reagent grade and used as received from the supplier.

Experimental methodology

The schematic representation of the ultrasonic horn-based setup for small-scale experiments has been shown in Fig. 2. Ultrasonic horn obtained from Dakshin, Mumbai, with a frequency of 20 kHz and a tip diameter of 1.2 cm, was used for all the laboratory scale studies. In our earlier work, the duty cycle of around 70% was found to be optimum for degrading dyes (Mahendran & Gogate, 2021) and hence the 70% duty cycle was maintained constant for all the experiments in the current study. Degradation of Acid Red 131 was carried out using a 200 mL solution for a treatment time of 3 h using the individual treatments of US, S- TiO_2 , H_2O_2 , and KPS and their combined treatment approaches. The variation of degradation with time was noted for each set of operating parameters, and the optimum parameter values were successfully determined. For each set of experiments, samples were withdrawn every 20 min over the total treatment period of 3 h. The absorbance of each sample was measured at a wavelength corresponding to the maximum absorbance of the dye (548 nm) using a UV-spectrophotometer and the concentration of the dye was determined from a calibration curve established using solutions of known concentrations. All the experiments were repeated to confirm the reproducibility of the data, and the errors were within $\pm 2\%$ of the average results reported in the discussion.

For photocatalysis experiments, the reactor (material of construction as borosilicate glass) setup was kept within a black box with two UV lights (Model: Philips TUV 8W, wavelength of 254 nm) attached to the two opposite walls (Fig. 2). The UV light intensity of two 8 W UV lamps inside the reactor was measured in our previous study as 240 ± 2 Lux, which is equivalent to 1.89×10^{-6} Einstein $\text{L}^{-1} \text{s}^{-1}$ (Agarkoti et al., 2023). The measured intensity clearly confirms that the borosilicate glass used as material of construction for the reactor is not completely absorbing the incident UV irradiations. Watzke and Kloss (1996) indeed reported that borosilicate glass is known to be 80% transparent to the UV irradiation of 254 nm wavelength. The setup was enclosed properly to avoid any leakage of UV light. The temperature

Fig. 2 Schematic representation of reactor setup for sonophotocatalysis experiments



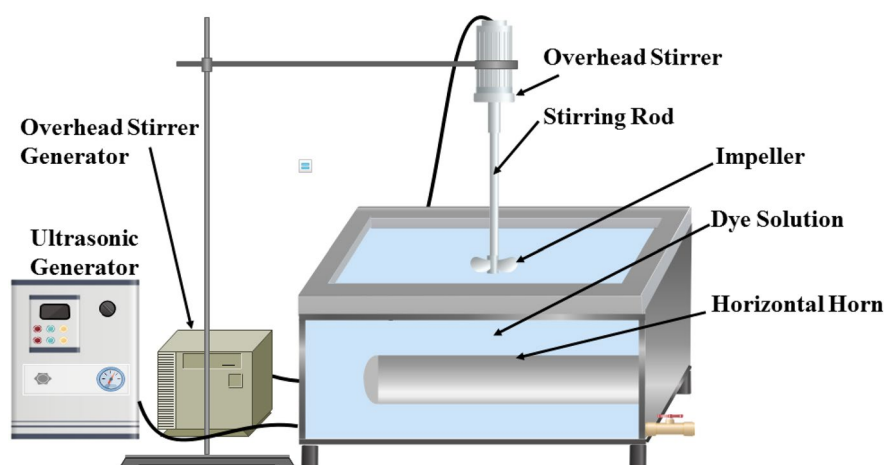
during the photocatalysis was maintained between 30–35 °C by adding ice cubes to the water bath at regular intervals.

Sulphur-doped titanium dioxide (S-TiO₂) was used for the degradation of AR131 using photocatalysis and the combination approach of US and UV light (8 W×2 tubes). The excitation of S-TiO₂ using the UV light of wavelength as 254 nm has been confirmed in the literature (Hussain et al., 2012; Xie et al., 2017). In the current work, the catalyst was synthesized by varying sulphur-to-titanium ratios (1:1, 2:1, and 3:1) and used at varying dosages of 100, 200, 300, and 400 ppm for the degradation of AR131. The

effectiveness of sulphur doping was examined by degrading AR131 using undoped TiO₂ at a similar optimum dosage of S-TiO₂. The same power of UV light (8 W×2 tubes) and mixing speed of 950 rpm were maintained, which was equivalent to the power dissipation of an ultrasonic horn (40,180 W/m³).

The large-scale applicability of the degradation schemes was examined using an ultrasonic reactor (US reactor) with a maximum capacity of 8 L equipped with a longitudinal horn of 24 cm length and a 3 cm tip diameter (Fig. 3). The US power and duty cycle were kept fixed at 1000 W and 70%, respectively. During the experiments, 3 L of synthetic

Fig. 3 Schematic representation of large-scale ultrasonic reactor



dye solution was treated under optimum conditions of initial concentration, pH, the dosage of photocatalyst, and chemical oxidants as established using the small-scale study. During the experiments involving the photocatalysts, two UV lights (Philips TUV 8W) were attached to the wooden lid of the reactor at the top. Total degradation time and sampling intervals were kept similar to the small-scale studies. The calorimetric efficiency of small-scale and large-scale horns was 8.2% and 11.3%, respectively, such that the power dissipated per unit volume for large-scale operations was 37.67 W/L and for small-scale operations it was 57.4 W/L.

Sonochemical synthesis of pure TiO₂ and sulphur-doped TiO₂ photocatalysts

The sonochemical synthesis of TiO₂ and S-TiO₂ photocatalysts was achieved utilizing the ultrasound-assisted technique. An ultrasonic bath was used instead of an ultrasonic horn, since tip erosion may occur in the case of a horn, which leads to impurities in the synthesized catalyst. The transducers are attached to the reactor base for bath-type reactors, and no direct contact between the solution and the transducer occurs (Agarkoti et al., 2021). The solution was taken in a glass reactor immersed in a coupling fluid (water), which makes the sonochemical activity generation typically due to the indirect mode. This approach is suitable for applications requiring lower intensities, such as the mixing of solutions or deagglomeration.

For the preparation of pure TiO₂, 10 ml of titanium isopropoxide was mixed with 2 ml of acetone and 2 ml of methanol in a reactor (250 ml beaker) which was then immersed in the ultrasonic bath. The titanium solution was sonicated at a power of 140 W and 70% duty cycle for 5 min. Subsequently, 50 ml of NaOH solution was added dropwise when a white precipitate was formed. Further sonication was performed for 30 min after the addition of the NaOH solution. The sonicated solution was then kept undisturbed, followed by filtration, and the precipitate obtained was dried and calcinated for three hours at 450 °C.

For the preparation of S-TiO₂, titanium isopropoxide (10 ml) was slowly added to the mixture of thiourea (a sulphur precursor) and ethanol (200 ml)

taken in the same reactor. The molar ratios of titanium isopropoxide and thiourea were varied as 1:1, 1:2, and 1:3. Due to the ultrasonic effect, rapid micromixing occurred and high temperatures were generated from intense bubble collapse, which can affect the process of catalyst synthesis favourably. Mixing was allowed for one hour and then the solvent was completely evaporated under reduced pressure using a rotary evaporator. After evaporation of ethanol, white powder was obtained and calcined at 500 °C for six hours under aeration. A yellow powder of S-TiO₂ was obtained as a final product after calcination.

Characterization of photocatalysts

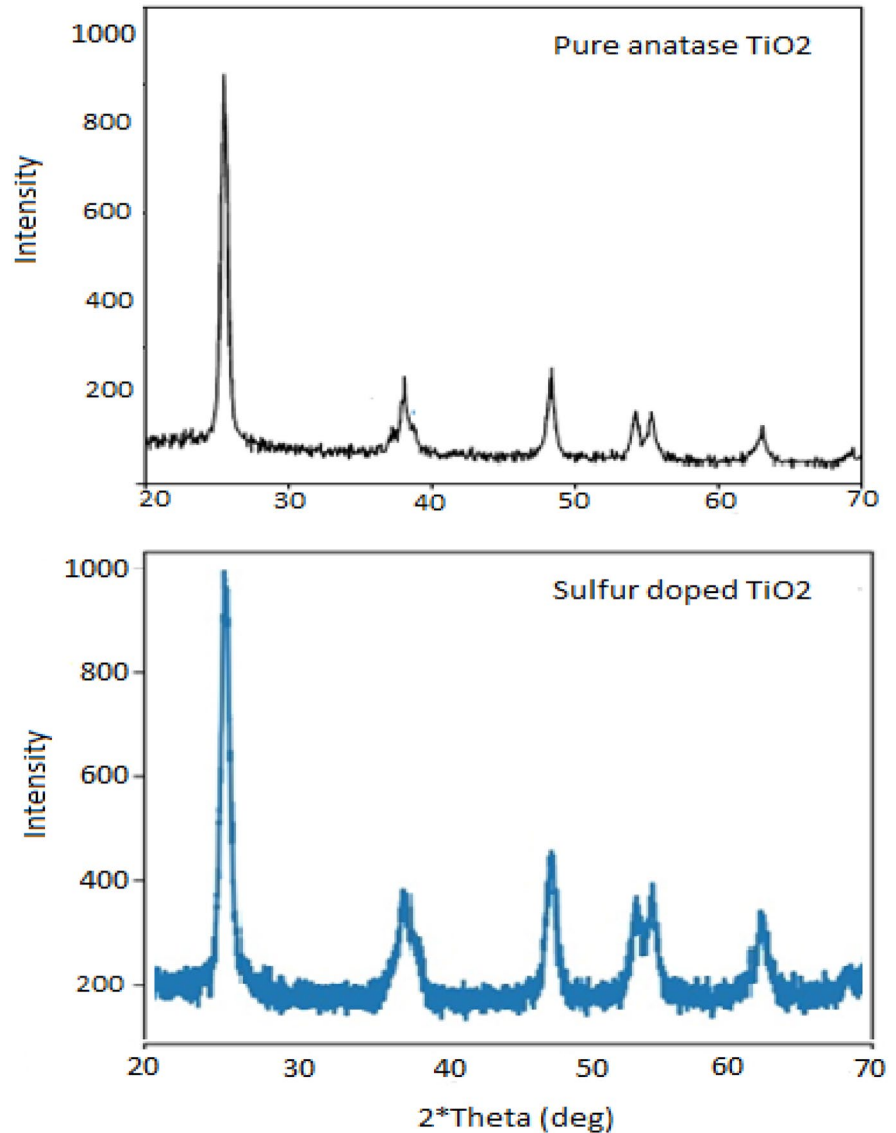
Pure TiO₂ and S-TiO₂ were characterized using X-Ray Diffractometer (XRD) analysis to determine the crystallographic structure of the photocatalysts. The operating conditions were set at a voltage of 40 kV and a current of 30 mA. The XRD patterns were recorded in the 2θ range of 10°–80° with a scan speed of 2°/min, a sampling pitch of 0.02° and a pre-set time of 0.6 s. FTIR analysis was also carried out for the sulphur-doped TiO₂ catalyst to confirm the presence of sulphur in the crystal lattice. The FTIR analysis identifies the presence of inorganic, organic, and polymeric compounds in the test material based on infrared light over the range of 10,000 to 100 cm⁻¹. For Dynamic Light scattering (DLS) analysis to quantify the size distribution of the S-TiO₂ photocatalyst, 100–200 μL of highly concentrated solution was taken and diluted to 1–2 mL in a microcuvette using ultrapure water. The obtained Z average value from DLS analysis is the mean value of the hydrodynamic diameters of the particles.

Results and discussions

Characterization of best performing photocatalyst

The characterization of the S-TiO₂ (S:Ti=2:1) having the best performance in the preliminary studies was performed using XRD, FTIR, and DLS analysis. The main peaks of XRD (Fig. 4) were observed to be present at 2θ=25.44°, 37.78°, 48.12°, 55.12°, and 62.62° for the S-TiO₂ whereas for pure TiO₂, the peak positions were present at 2θ=25.51°, 36.96°, 48.91°, 54.76°, and 62.4°. It was observed that the peak

Fig. 4 XRD analysis of pure TiO_2 and S- TiO_2 (S:Ti=2:1)



positions were nearly the same for both pure TiO_2 and S- TiO_2 , which means that doping did not change the crystalline structure of the photocatalyst. The peak positions also showed that the S- TiO_2 is crystalline in nature with anatase as the major phase based on the strong diffraction peaks observed at 25.44° and 48.12° (Thamaphat et al., 2008). The crystallite sizes of pure TiO_2 and S- TiO_2 photocatalysts were determined from the Scherrer equation. The shape factor (k) was considered as 0.89, and the wavelength of the X-ray (λ) was considered 1.5406 nm. The full width of maximum intensity (β) for pure TiO_2

and sulphur-doped TiO_2 was obtained as 0.0196 and 0.0208 radians, respectively. The average crystallite sizes of the pure TiO_2 and S- TiO_2 photocatalysts were 71.73 nm and 67.58 nm, respectively. Nam et al. (2012) also reported an average S- TiO_2 crystal size of ~ 50 nm in diameter, which is close to the size obtained in the current study.

The FTIR spectra in the range of 500 cm^{-1} to 2750 cm^{-1} were studied, and the results are shown in Fig. 5. At 1629.85 cm^{-1} , the peak was observed due to the surface-adsorbed hydroxyl groups. The peak originated from the O–H bending vibration of

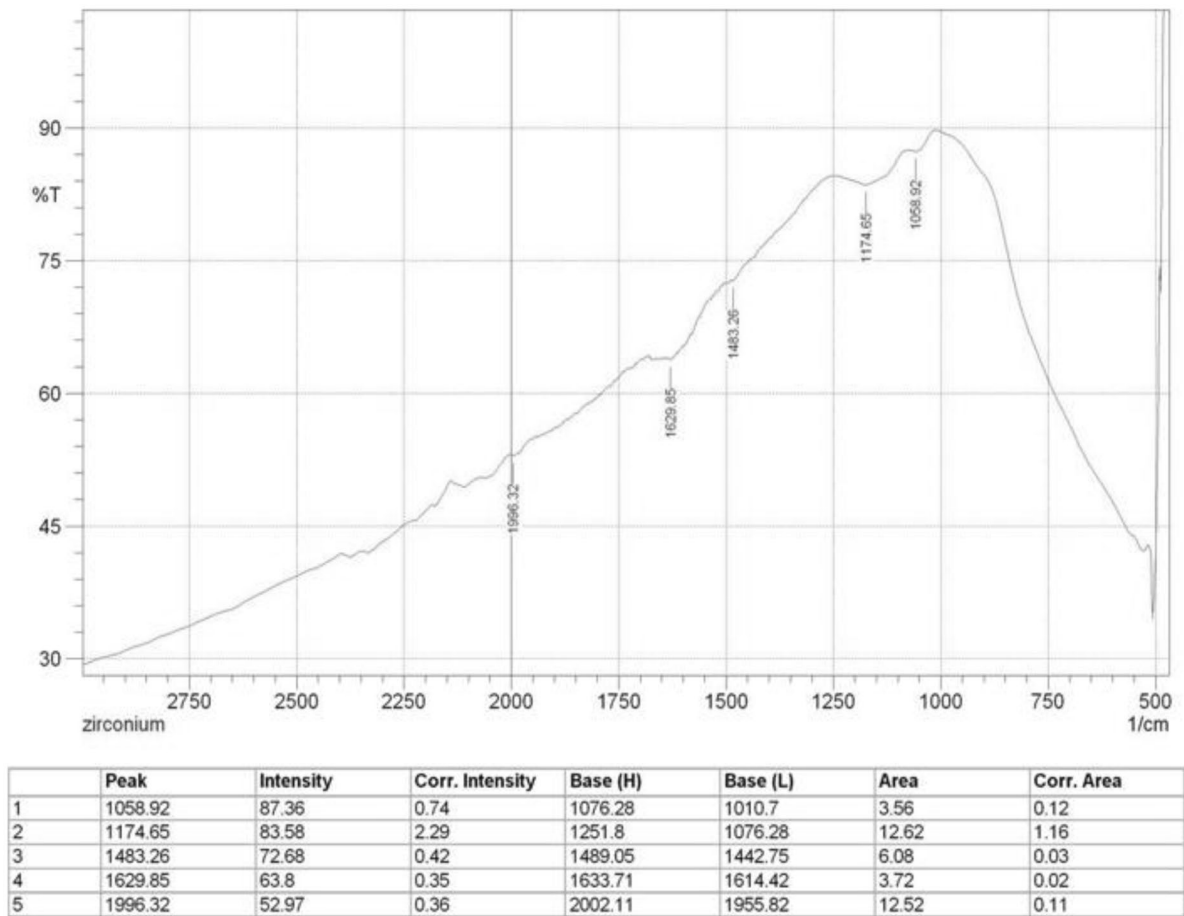


Fig. 5 FTIR analysis of S-TiO₂ (S:Ti=2:1)

physisorbed/chemisorbed water molecules on the catalyst surface. The peak at 1058.92 cm⁻¹ originated from the vibration of the Ti-O-S bond and thus confirmed the incorporation of sulphur into the TiO₂ lattice. Another peak at 1174.65 cm⁻¹ corresponded to S-O vibration, confirming the coordination of bidentate SO₄²⁻ ions to Ti⁴⁺ ions.

The dynamic light scattering (DLS) method was applied to perform the particle size distribution analysis. The number distribution showed the count of particles in different-size bins (Fig. 6). A first power relationship existed between each particle size and its contribution to distribution. From our analysis, the photocatalyst sample’s most predominant size was 236 nm, whereas the average particle size was 573 nm.

Effect of initial concentration on the dye degradation

Initial concentration is attributed as an important parameter deciding the efficacy of dye degradation. Generally, the degradation decreases with an increase in the initial concentration, typically after an optimum, attributed to a fixed number of •OH radicals generated that cannot react efficiently with higher concentrations of the pollutant (Rajoriya et al., 2016). Thus, optimum selection of the initial concentration strongly depends on the availability of •OH radicals decided by the generation and subsequent utilization.

The effect of initial concentration on dye degradation was studied at different initial concentration

			Size (d.nm):	% Number:	St Dev (d.n...
Z-Average (d.nm):	572.9	Peak 1:	236.6	99.8	51.94
Pdl:	0.722	Peak 2:	1016	0.2	166.0
Intercept:	1.07	Peak 3:	0.000	0.0	0.000

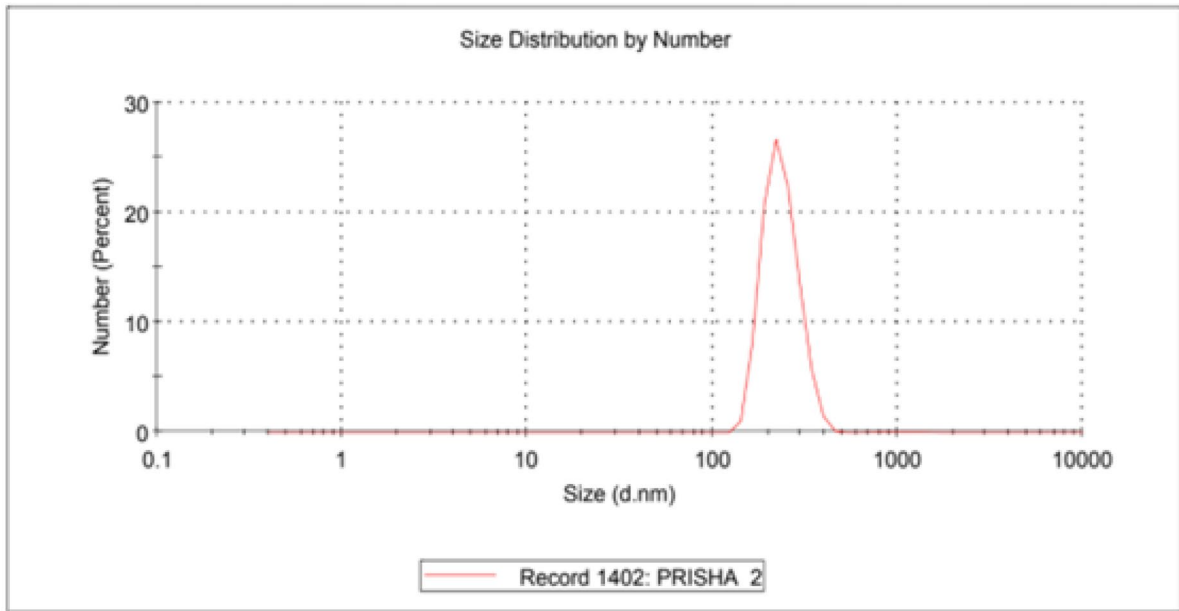
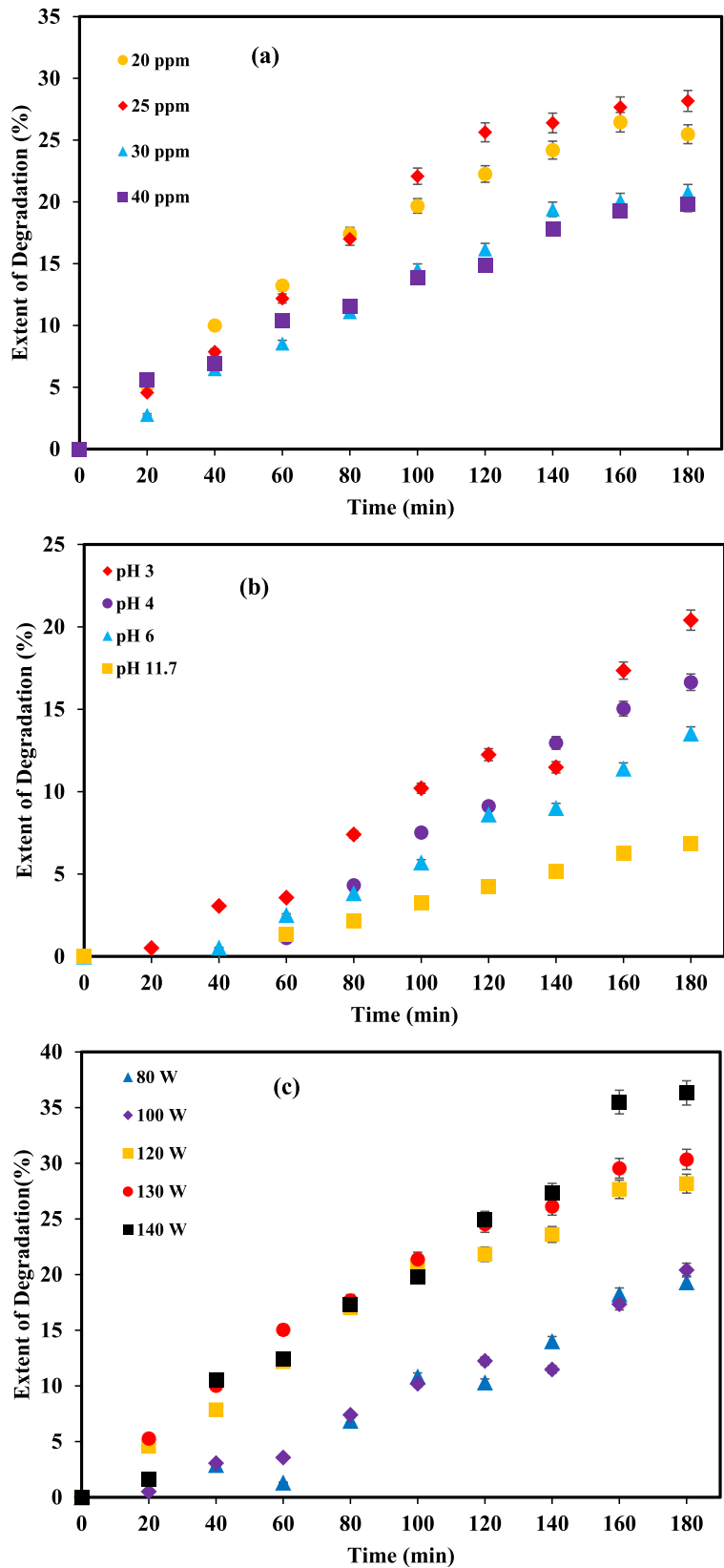


Fig. 6 DLS analysis of S-TiO₂ (S:Ti = 2:1)

values as 20, 25, 30, and 40 ppm at fixed pH of 3. It was observed that 20 and 25 ppm as the initial concentration showed a marginal degradation change with actual values of 25.48% and 28.17%, respectively. A subsequent increase in the initial concentration to 30 and 40 ppm decreased the extent of degradation to 20.79% and 19.80%, respectively (Fig. 7a). Based on the results, an initial concentration of 25 ppm with the maximum extent of degradation was taken as the optimum and used in further degradation studies. Using cavitation, the pollutant molecules undergo decomposition by two methods viz. thermal pyrolysis and free radical attack. The number of bubbles generated and the quantum of •OH radicals produced remain constant at a constant cavitation condition. With increasing dye concentration in the solution initially, the possibility of dye molecules being entrapped in a radical environment increases. Hence, their chance of getting attacked by the •OH

radicals increase, due to which the overall degraded substrate shows an increase. Thus, the extent of degradation increases with increasing initial concentration (Alkaykh et al., 2020). But after exceeding a certain initial concentration of the dye, the number of •OH radicals may not be sufficient for oxidizing the dye molecules to a higher extent. Due to the unavailability of •OH radicals for larger concentrations of dye, the extent of degradation again shows a drop beyond the optimum. Similar trends are seen in the literature although with different or no existence of an optimum depending on the range of concentrations studied. (Rajoriya et al., 2017) reported that an increase in the initial concentration from 30 to 60 ppm resulted in a reduction in the degradation of reactive blue 13 from 47 to 19%. Zampeta et al. (2021) also observed a decrease in the degradation efficacy at a higher initial concentration when treated with HC + 1 gL⁻¹ H₂O₂. The results showed that the degradation extent of Black, Red, Green, and

Fig. 7 Effect of operating parameters on decolourization behaviour of AR131 (a) initial concentration, (b) pH, and (c) ultrasonic power



Cyan dye decreased from 52.9 to 45.7%, 22.7 to 9.7%, 47.7 to 29.7%, and 47.6 to 23.2%, respectively, as the initial concentration of the dyes changed from 0.3 to 0.6 as the optical density. The selection of an optimum concentration dependent on the specific contaminant in question is thus required so as to achieve higher degradation.

Effect of pH on the degradation of dye

The effect of pH on the extent of degradation was determined by taking 25 ppm as the initial concentration of dye solution and performing sonication at varying pH values of 3, 4, 6, and 11.7. The operating power of the ultrasonic horn and duty cycle were kept constant at 100 W and 70%, respectively. The results (Fig. 7b) revealed that maximum degradation of 20.41% was obtained at an acidic pH of 3 within 3 h, whereas, 16.64%, 13.53%, and 6.83% degradation were observed at pH values of 4, 6, and 11.7, respectively. The change in pH of the dye solution significantly influenced the extent of AR131 degradation. The acidic pH was observed to be more efficient than the basic pH, as the AR131 dye is predominantly present in molecular form at the lower pH values (Fedorov et al., 2022). Due to hydrophobicity in the molecular form, they get inhabited at the liquid–gas interface of the collapsing cavities. Consequently, the entrapped dye molecules first experience thermal decomposition and later are attacked by the $\bullet\text{OH}$ radicals generated by cavity collapse and present at high concentrations, thereby enhancing the degradation rate.

On the other hand, at a basic pH, the dye molecules are in the ionized state, and due to their hydrophilic properties, they get inhabited in the bulk of the liquid. In the bulk, the temperature is not very high, and the concentration of $\bullet\text{OH}$ radicals is lower as only a few $\bullet\text{OH}$ radicals migrate to the bulk, thereby decreasing the extent of oxidation of dye molecules (Saharan et al., 2011). Therefore, based on the maximum degradation, pH 3 was taken as the optimum pH value and was used in further studies. Suresh Kumar et al. (2017) also reported that the degradation extent of MB (methylene blue) dye by HC increased at acidic conditions (pH below 5) with a maximum degradation of 32.32% at pH 2, which was quite high compared to 3.89% at pH 10. Kumar et al. (2017) during the

decolourization of methylene blue observed that, at pH 2, maximum decolourization (32.32%) occurred whereas pH 10 showed the least (3.896%) degradation. Quantitative differences in the best pH elucidate the importance of the present study for AR131.

Effect of ultrasonic power on the dye degradation

As the input power increases, the energy supplied and available for cavitation also increases, which results in an enhanced quantum of cavitation events. In addition, the oscillation and collapse of the cavities become more violent with the increase in input power, which gives rise to a greater amount of $\bullet\text{OH}$ radicals. Also, the thermal pyrolysis of dye molecules becomes easier at higher supplied energy due to higher cavitation activity. Therefore, the degradation can increase with an increase in input power. The trend, however, cannot be generalized for all ultrasonic devices, as sometimes an optimum operating power is observed. At much higher input power levels, the excess supplied energy leads to excessive cavities, yielding cushioning and decoupling effects that consequently result in the lowering of cavitation collapse intensity and hence the pollutant degradation.

For determining the effect of ultrasonic power, various operating powers of 80, 100, 120, 130, and 140 W were applied at pH of 3 and 25 ppm as initial concentration. Maximum degradation of 19.31%, 20.41%, 28.17%, 30.34%, and 36.31% was observed for input power of 80 W, 100 W, 120 W, 130 W, and 140 W respectively, after 180 min of treatment (Fig. 7c). A marginal difference in degradation extent was observed for 80 and 100 W of power however, degradation extent at 140 W was the maximum, and hence it was used in further studies. An increasing trend of degradation with increasing ultrasonic power was also observed by Soumia and Petrier (2016) for the degradation of cresol red, where the degradation extent increased (almost 52% to 95%) continuously with an increase in ultrasonic power from 20 to 80 W. (Böbl et al., 2023) studied the degradation of RhB dye at various acoustic powers in the presence/absence of BF-KBT-PT piezocatalyst and reported 84%/79% degradation at 68 W/L and 94%/92% at 90 W/L. Different quantitative dependency of the degradation of dyes on ultrasonic power confirm the significance of current work.

Effect of H₂O₂ Addition on dye degradation using US

To determine the effect of H₂O₂ on the degradation extent of AR131, studies were performed at varying dosages of 50, 100, and 500 ppm at the optimum conditions of 25 ppm as the initial concentration of dye, a pH of 3, and 140 W as the ultrasonic power. It was observed that the use of 50 ppm and 100 ppm H₂O₂ dosages increased the degradation extent, whereas at 500 ppm a lower extent of degradation was observed (Fig. 8). A maximum degradation of 40.14% was observed when the dosage of H₂O₂ was 100 ppm. The individual approach of H₂O₂ for the degradation of AR131 resulted in a maximum degradation of 21.05%, which is lower compared to the US combined with H₂O₂. The reason for higher degradation with the addition of H₂O₂ at 100 ppm was the enhanced generation of •OH radicals by the hydrogen peroxide dissociation due to the cavitational activities, thereby increasing the extent of degradation. Beyond the optimum concentration of 100 ppm, any excess dosage of H₂O₂ acts as a radical scavenger, and the recombination reactions of •OH radicals are quite prevalent. Indeed, a similar trend, although with different optimum values, has been elucidated by Kumar et al. (2017), Rajoriya et al. (2017), Gore et al. (2014), and Wang et al. (2019) for the degradation of Methylene Blue,

Reactive Blue 13, Reactive Orange 4 and Rhodamine B respectively. Overall, it was confirmed that different optimum concentrations of H₂O₂ exist beyond which degradation extent decreases upon a further increase in H₂O₂ dosage.

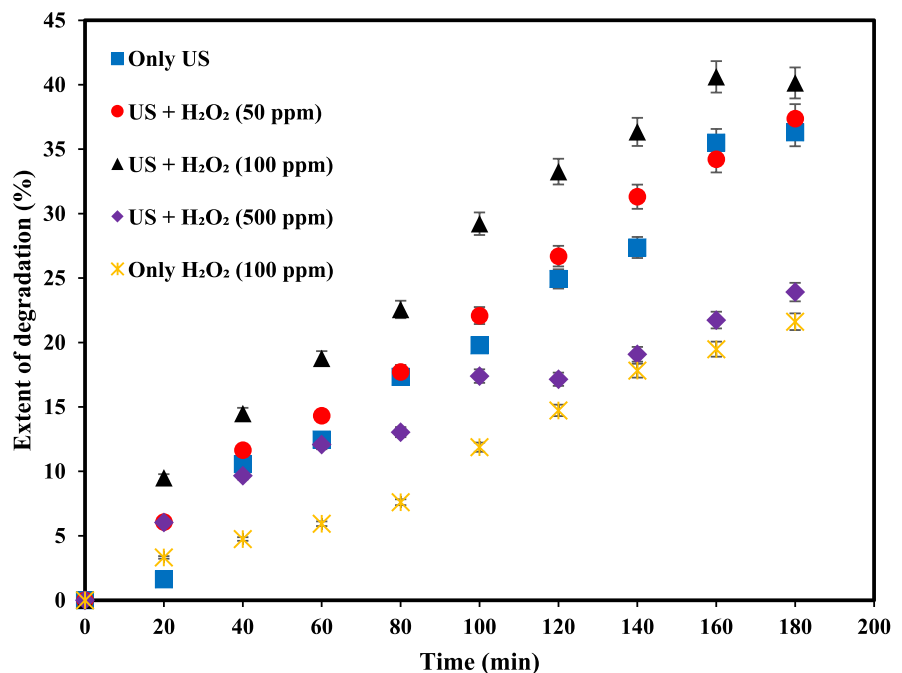
Pseudo-first-order kinetic model was used for the determination of rate constants at different H₂O₂ dosages by plotting -ln(C/C₀) vs time. The synergy between US and H₂O₂ was also determined using the rate constants achieved for the AR131 degradation using the individual US and H₂O₂ (in the presence of stirring) and the US+H₂O₂ combination approach at optimum loading.

The synergistic coefficient was determined as:

$$f_{(US+H_2O_2)} = \frac{K_{(US+H_2O_2)}}{K_{(US)} + K_{(H_2O_2)}} = \frac{0.0032 \text{ min}^{-1}}{0.0025 \text{ min}^{-1} + 0.0013 \text{ min}^{-1}} = 0.8421 \quad (1)$$

The value of the synergistic coefficient suggests an absence of synergy in the combined US/H₂O₂ system. Wu (2007) also observed no synergy between US and H₂O₂ attributed to the fact that most of the H₂O₂ might be present in bulk instead of within cavitation bubbles owing to its high solubility in water

Fig. 8 Decolourization behaviour of AR131 with varying H₂O₂ dosage



and low volatility. Voncina and Majcen-Le-Marechal (2003) suggested in their studies that the effect of H_2O_2 on degradation extent depends on the type of pollutant being studied, as in their case the concentration of all dyes decreased by more than 91%, however, the concentration of some of the dyes decreased only after a treatment period of 4 h. Dukkanci and Gündüz (2006), Manousaki et al. (2004), Goel et al. (2004) also observed the absence of any positive synergy between ultrasound and H_2O_2 whereas, Patil et al. (2021a, b) observed a good synergistic coefficient (2.04) between ultrasound and H_2O_2 for the degradation of thiamethoxam. Raut-Jadhav et al. (2016) also observed a high synergistic coefficient (25.74) between ultrasound and H_2O_2 during the degradation of methomyl (carbamate group pesticide). Therefore, it is important to understand that the influence of H_2O_2 is typically dependent on the pollutant type, which makes our study quite important.

Effect of catalyst dosage on the dye degradation using US and UV

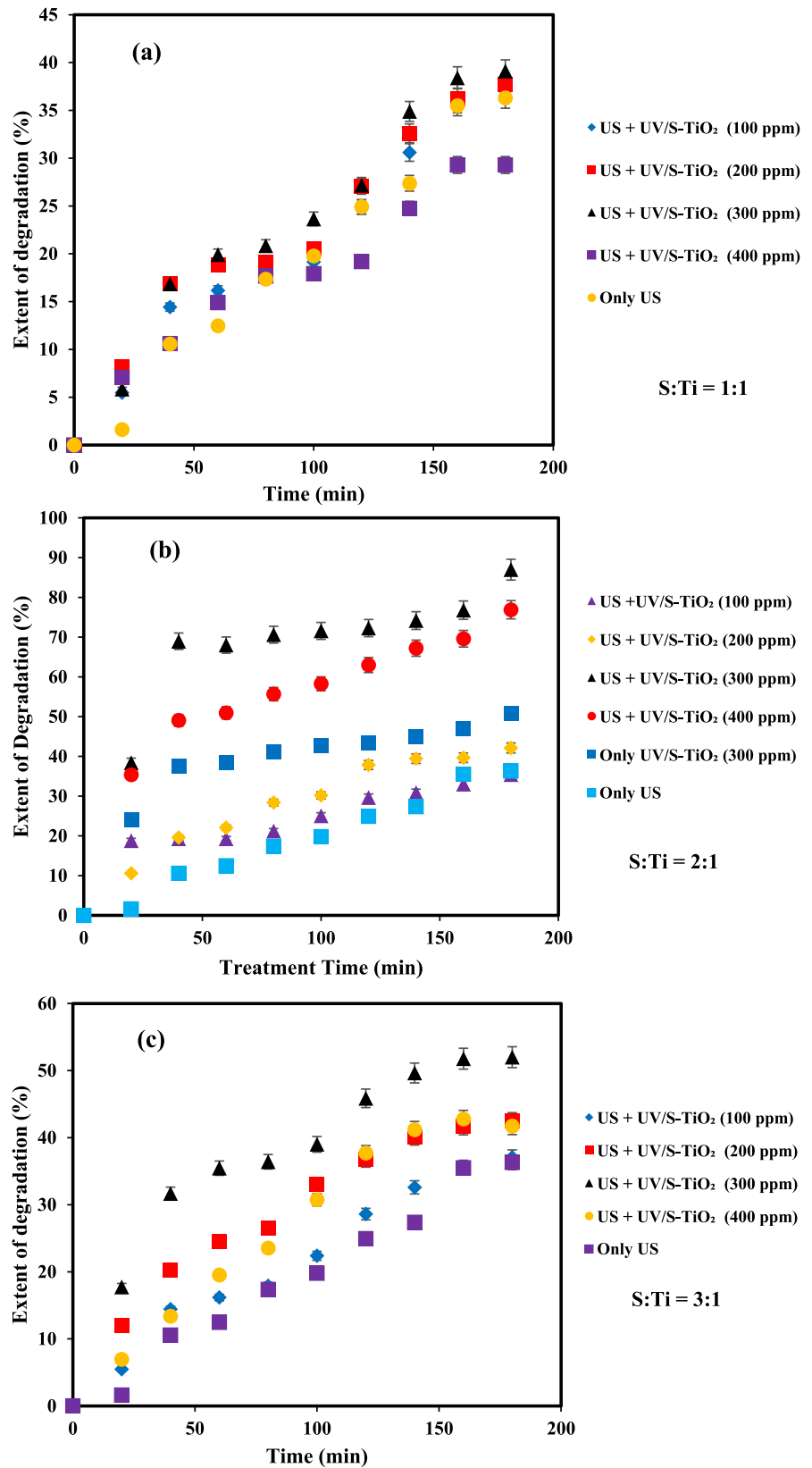
The degradation of AR131 was studied using the synthesized S-TiO₂ at various S:Ti ratios of 1:1, 2:1, and 3:1 at 100, 200, 300, and 400 ppm of dosages, respectively. Figure 9a-c represent the degradation behaviour with varying S-TiO₂ dosage at the different S:Ti ratios (1:1, 2:1, and 3:1, respectively). The extent of AR131 degradation increased from 100 to 300 ppm, as the catalyst dosage increased, however, above 300 ppm, the degradation did not increase with a further rise in the S-TiO₂ dosage for all the S:Ti ratios. Therefore, the S-TiO₂ dosage of 300 ppm was considered the optimum. For the S-TiO₂ dosages of 100 and 200 ppm, the decolourization behaviour was not well distinguished regarding the variation in S:Ti ratio. However, for the S-TiO₂ dosage of 300 and 400 ppm, the degradation extent exhibited a clear deviation with the varying S:Ti ratio. The most efficient ratio established was 2:1 with a maximum degradation of 86.97% at 300 ppm of S-TiO₂ dosage. The higher extent of AR131 degradation using S-TiO₂ was attributed to the enhanced generation of •OH radicals through the electron-hole pairs (Piałkowska et al., 2021) present in an optimum amount as well as the additional nuclei provided by the catalyst for the cavitation inception (Agarkoti et al., 2022). The doping of sulphur to the TiO₂ typically lowered its band gap in comparison to the undoped TiO₂,

which consequently enhanced the promotion of electrons from the valence band to the conduction band, forming the electron-hole pairs. The band gap of the S-TiO₂ has been reported as 1.7 eV which is lower than that for the TiO₂ with a band gap of 3.2 eV (Humayun et al., 2018). In the case of undoped TiO₂, both conduction band (CB) and valence band (VB) contains Ti 3*d* and O 2*p* orbitals. Ti 3*d* orbital breaks into two states (*t_{2g}* and *e_g*) which divides the CB into upper and lower fragments. However, in the case of S-TiO₂, the S 3*p* are slightly delocalized which significantly promote the generation of VB with Ti 3*d* and O 2*p* states. Subsequently, the involvement of S 3*p* states with VB enhances the width of VB, which leads to the reduction in the band gap energy of the S-TiO₂ (Umebayashi et al., 2002). The proposed kinetic mechanism has been shown in Fig. 10. The formed electron-hole pair leads to the generation of •OH radicals by reducing the H₂O molecule adsorbed on the catalyst surface (Khan et al., 2017). In addition, the presence of the US improved the mass transfer rate and also acted as a medium for catalyst cleaning (Duan et al., 2020). The increase in the mass transfer rate increased the probability of the H₂O molecules contacting the catalyst surface, thereby enhancing the rate of generation of •OH radicals. These advocated effects are dominant until an optimum dosage of S-TiO₂ as above this dosage the interaction between S-TiO₂ and UV light would get hindered due to the excess S-TiO₂ photocatalysts (Gaya & Abdullah, 2008), and additionally the cavities would not be able to acquire the maximum size for the efficient collapse.

Dhanke and Wagh (2020) applied varied TiO₂ dosage of 100, 200, 300, and 400 ppm during the degradation of Acid Red 18 and obtained 300 ppm as the optimum at which the maximum degradation achieved was 88.1% after 150 min. Similarly, Wang et al. (2011) also confirmed the presence of an optimum loading of TiO₂ (100 mg/L) at which the maximum degradation of 98.8% was achieved for Reactive Red 2 dye. Therefore, the optimization of both TiO₂ dosage and S:Ti ratio needs to be successfully established for the maximum degradation of a pollutant as well as for the prevention of excess TiO₂ usage.

The best performing S:Ti ratio (2:1) for S-TiO₂ was used for the degradation studies using individual approaches and was considered for the estimation of the kinetic parameters. Only 50.87% as the AR131 degradation was achieved using the individual approach of UV/S-TiO₂ (300 ppm dosage, S:Ti

Fig. 9 Decolourization behaviour of AR131 with varying TiO₂ dosage (a) S:Ti = 1:1, (b) S:Ti = 2:1, and (c) S:Ti = 3:1



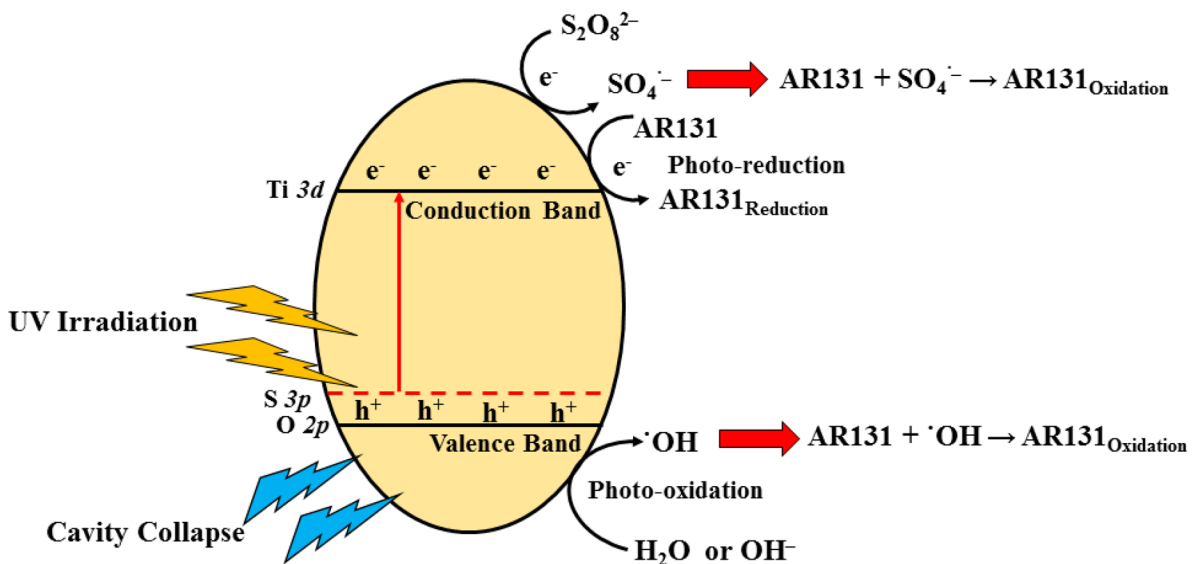


Fig. 10 Kinetic mechanism for the photo-activation of the S-TiO₂

ratio of 2:1). The enhancement in degradation using US+UV/S-TiO₂ compared to individual US and UV/S-TiO₂ was determined on the basis of the synergistic coefficient as follows:

$$f_{(US+UV/S-TiO_2)} = \frac{K_{(US+UV/S-TiO_2)}}{K_{(US)} + K_{(UV/S-TiO_2)}} = \frac{0.0113 \text{ min}^{-1}}{0.0025 \text{ min}^{-1} + 0.0047 \text{ min}^{-1}} = 1.5694 \quad (2)$$

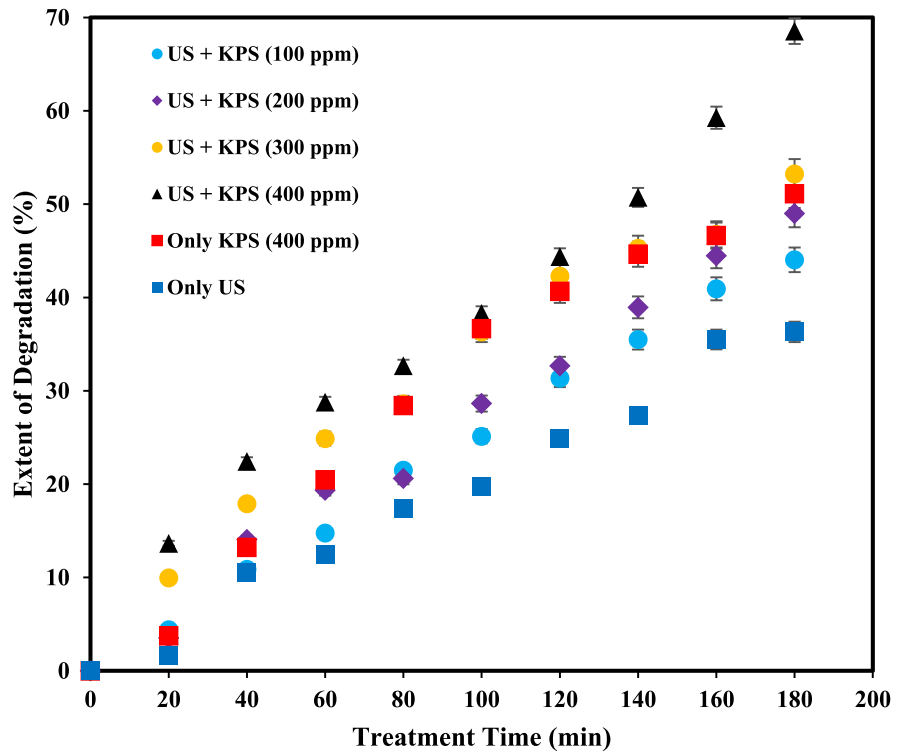
The value of the synergistic coefficient demonstrates that the rate constant of the combined approach of US+UV/S-TiO₂ was higher than the sum of the individual rate constants. Mosleh et al. (2016) also obtained a synergistic coefficient of 2.23 during the sonophotocatalytic degradation of trypan blue and vesuvine dyes using a blue light-activated photocatalyst. Benomara et al. (2021) observed a synergistic coefficient of 1.33 during the sonophotolytic degradation of Methyl Violet 2B. It was advocated that the high magnitude of turbulence and the prevention of agglomeration of suspended catalyst particles in the presence of US was responsible for the increase in catalyst surface area and improvement in the generation of active free radicals. Kumar et al. (2017) observed a synergistic coefficient of 1.46 for the degradation of Methylene Blue using Bi-doped TiO₂. Caliskan et al. (2017) observed that for the

degradation of Reactive Red 180, synergistic coefficients for COD and TOC removal were 1.48 and 1.17, respectively. Similarly, Kumar et al. (2018) observed the synergistic coefficient to be 2.11 during the degradation of ternary dyes (Methylene Blue, Methyl Orange, Rhodamine B). The differences in the synergistic coefficients as a function of the pollutant again confirm the importance of the current work.

Effect of KPS addition on dye degradation using US

The effect of KPS addition on degradation was investigated using US combined with varying KPS dosages of 100, 200, 300, and 400 ppm, respectively. The AR131 degradation was observed to increase monotonously with an increase in the dosage of KPS, with degradation of 44.04%, 48.99%, 53.23%, and 68.58% observed at KPS dosages of 100, 200, 300, and 400 ppm, respectively, at an optimum power of 140 W, pH of 3, and a time period of 3 h (Fig. 11). The maximum degradation of 68.54% was observed when the KPS loading was 400 ppm, which was thereby chosen as the best for AR131 degradation. However, the individual approach of KPS for the degradation of AR131 resulted in only 51.12% degradation. The increase in the extent of degradation with increasing KPS dosage was attributed to the generation of a higher quantum of •OH and SO₄•⁻

Fig. 11 Decolourization behaviour of AR131 with varying KPS dosage



radicals under the influence of cavitation (Agarkoti et al., 2021). Importantly, no scavenging effect was seen at a higher dosage, however, optimum loading is entirely dependent on the nature of the pollutant, and an optimization studies for KPS dosage are always needed for individual substrates to understand the effect of KPS on their degradation, elucidating the importance of the work. Daware and Gogate (2021) studied the degradation of 2-Picoline using US combined with KPS and reported an increasing trend of degradation for the variation in KPS dosage from 4 to 20 ppm. However, a further increases in KPS dosage above 20 ppm reduced the degradation extent marginally. The reduced degradation at much higher loading was explained by the scavenging action of SO_4^- radicals by excess $S_2O_8^{2-}$ ions. Patil and Shukla (2015) also observed a similar trend for the degradation of Reactive Yellow dye, where the degradation increased from 0.7 (43.2%) to 3.7 mM (93.2%) and decreased with an increase in the loading to 4.4 mM (80.9%). More and Gogate (2018) observed a monotonous increase in degumming extent for the US-assisted KPS treatment of crude soybean oil from 0.6 (88.99%) to 2 g/L (94.08%), however, with a further increase in loading to 5 g/L, the degradation extent

remained constant at 94.08%. Within the range of KPS loading studied in their work, the existence of any scavenging effect with increasing dosage of KPS was not observed, and 400 ppm as KPS dosage was used in subsequent studies.

The pseudo-first-order reaction rate constants at various dosages of KPS were determined by plotting $-\ln(C/C_0)$ vs time. For quantification of the efficiency of the combined process (US+KPS), the synergistic coefficient was determined as follows:

$$\begin{aligned}
 f_{(US+KPS)} &= \frac{K_{(US+KPS)}}{K_{(US)} + K_{(KPS)}} \\
 &= \frac{0.0056 \text{ min}^{-1}}{0.0025 \text{ min}^{-1} + 0.0041 \text{ min}^{-1}} = 0.8484
 \end{aligned}
 \tag{3}$$

From the obtained synergistic coefficient, it can be concluded that although the combined approach resulted in a greater extent of degradation compared to the individual ones, the combined approach did not improve the rate constant above the sum of the rate constants of the individual approaches. The possible reason could be the lower affinity of the dye molecules towards the $SO_4^{\bullet-}$ radicals. Lakshmi et al. (2021) also observed the absence of synergy between

HC and KPS for the degradation of Acid Violet 7. The authors also stated that the lower reactivity of dye molecules towards $\text{SO}_4^{\bullet-}$ radicals could be the reason for the low synergistic coefficient (0.98). Thanekar and Gogate (2019) also obtained a low synergistic coefficient (0.89) using KPS during the treatment of real industrial effluent of organic pollutants. On the other hand, Daware and Gogate (2021) observed a high synergetic coefficient (2.9) among the US and KPS for the degradation of 2-Picoline. Thus, for each type of pollutant, a separate study is needed to confirm the effect of the specific intensifying agent, clearly demonstrating the significance of the current work.

Use of multiple oxidant based combination approaches:

The degradation of AR131 dye using the different combination approaches such as (a) $\text{US} + \text{H}_2\text{O}_2 + \text{KPS}$, (b) $\text{US} + \text{H}_2\text{O}_2 + \text{UV/S-TiO}_2$, (c) $\text{US} + \text{KPS} + \text{UV/S-TiO}_2$, and (d) $\text{US} + \text{H}_2\text{O}_2 + \text{KPS} + \text{UV/S-TiO}_2$ was studied at the optimized US parameters and optimum loadings of the oxidants and photocatalyst. Figure 12a shows that the combined approach of $\text{US} + \text{KPS} + \text{UV/S-TiO}_2$ showed the highest degradation efficacy with 90.3% degradation within 3 h, whereas the extent was lowest for the $\text{US} + \text{H}_2\text{O}_2 + \text{KPS}$ approach among the various combinations with only 56.73% degradation. The $\text{US} + \text{H}_2\text{O}_2 + \text{KPS}$ approach showed even lower efficacy than $\text{US} + \text{KPS}$, which was mainly due to the scavenging action of H_2O_2 . Similarly, the degradation extent of $\text{US} + \text{UV/S-TiO}_2$ and $\text{US} + \text{UV/S-TiO}_2/\text{KPS}$ also decreased with the addition of H_2O_2 by almost 18% and 10%, respectively. When more than one additive is present in the solution, their working mechanisms are not independent of each other. When the generated $\bullet\text{OH}$ radicals cross a certain critical concentration in the medium, their scavenging action prevails, and reaction kinetics shift towards recombination reactions, and hence the efficiency of degradation reduces (Agarkoti et al., 2021). In addition, H_2O_2 also contributes to scavenging action depending on the residual concentration values.

The pseudo-first-order reaction rate constants for the different combination approaches were determined by plotting $-\ln(C/C_0)$ vs time and were utilized for the determination of synergistic coefficients. The determination of the synergistic coefficients for different approaches has been now illustrated:

$$\begin{aligned} f_{(\text{US}+\text{H}_2\text{O}_2+\text{KPS})} &= \frac{K_{(\text{US}+\text{H}_2\text{O}_2+\text{KPS})}}{K_{(\text{US})} + K_{(\text{H}_2\text{O}_2)} + K_{(\text{KPS})}} \\ &= \frac{0.0042 \text{ min}^{-1}}{0.0025 \text{ min}^{-1} + 0.0013 \text{ min}^{-1} + 0.0041 \text{ min}^{-1}} = 0.5316 \end{aligned} \quad (4)$$

$$\begin{aligned} f_{(\text{US}+\text{H}_2\text{O}_2+\text{UV/S-TiO}_2)} &= \frac{K_{(\text{US}+\text{H}_2\text{O}_2+\text{UV/S-TiO}_2)}}{K_{(\text{US})} + K_{(\text{H}_2\text{O}_2)} + K_{(\text{UV/S-TiO}_2)}} \\ &= \frac{0.0088 \text{ min}^{-1}}{0.0025 \text{ min}^{-1} + 0.0013 \text{ min}^{-1} + 0.0047 \text{ min}^{-1}} = 1.0353 \end{aligned} \quad (5)$$

$$\begin{aligned} f_{(\text{US}+\text{KPS}+\text{UV/S-TiO}_2)} &= \frac{K_{(\text{US}+\text{KPS}+\text{UV/S-TiO}_2)}}{K_{(\text{US})} + K_{(\text{KPS})} + K_{(\text{UV/S-TiO}_2)}} \\ &= \frac{0.0121 \text{ min}^{-1}}{0.0025 \text{ min}^{-1} + 0.0041 \text{ min}^{-1} + 0.0047 \text{ min}^{-1}} = 1.0708 \end{aligned} \quad (6)$$

$$\begin{aligned} f_{(\text{US}+\text{H}_2\text{O}_2+\text{KPS}+\text{UV/S-TiO}_2)} &= \frac{K_{(\text{US}+\text{H}_2\text{O}_2+\text{KPS}+\text{UV/S-TiO}_2)}}{K_{(\text{US})} + K_{(\text{H}_2\text{O}_2)} + K_{(\text{KPS})} + K_{(\text{UV/S-TiO}_2)}} \\ &= \frac{0.0095 \text{ min}^{-1}}{0.0025 \text{ min}^{-1} + 0.0013 \text{ min}^{-1} + 0.0041 \text{ min}^{-1} + 0.0047 \text{ min}^{-1}} = 0.7540 \end{aligned} \quad (7)$$

In the previous section, it was established that no synergism was present in the combined approach of $\text{US} + \text{H}_2\text{O}_2$, and the calculations for other combined approaches of $\text{US} + \text{H}_2\text{O}_2 + \text{KPS}$, $\text{US} + \text{H}_2\text{O}_2 + \text{UV/S-TiO}_2$, and $\text{US} + \text{H}_2\text{O}_2 + \text{KPS} + \text{UV/S-TiO}_2$ also revealed that H_2O_2 addition did not improve the degradation extent. The synergetic coefficient was less than 1 or almost equal to 1 in all the H_2O_2 -assisted processes, which indicates that the H_2O_2 was ineffective in intensifying AR131 degradation. For the approach of $\text{US} + \text{KPS} + \text{UV/S-TiO}_2$, a synergetic coefficient with a value of 1.0708 was observed, although the value was not significantly high. The comparison revealed that $\text{US} + \text{KPS} + \text{UV/S-TiO}_2$ achieved the highest degradation extent of 90.3% with a synergistic coefficient of 1.0708 however, the highest synergistic coefficient was obtained for $\text{US} + \text{UV/S-TiO}_2$ with a value of 1.5694. Therefore, the combined approach of $\text{US} + \text{UV/S-TiO}_2$ was observed to be the most efficient for the degradation of AR131 in terms of synergy. The $\text{US} + \text{H}_2\text{O}_2$ and $\text{US} + \text{KPS}$ approaches increased the degradation extent compared to the individual US. However, H_2O_2 and KPS did not display any significant synergy when introduced into combined approaches. Karami et al. (2016) observed that for the degradation of Reactive Red 198, $\text{O}_3/\text{H}_2\text{O}_2/\text{US}$ process was the most promising combination scheme (100% colour removal and 69% COD removal after 40 min of reaction time). Gogate and

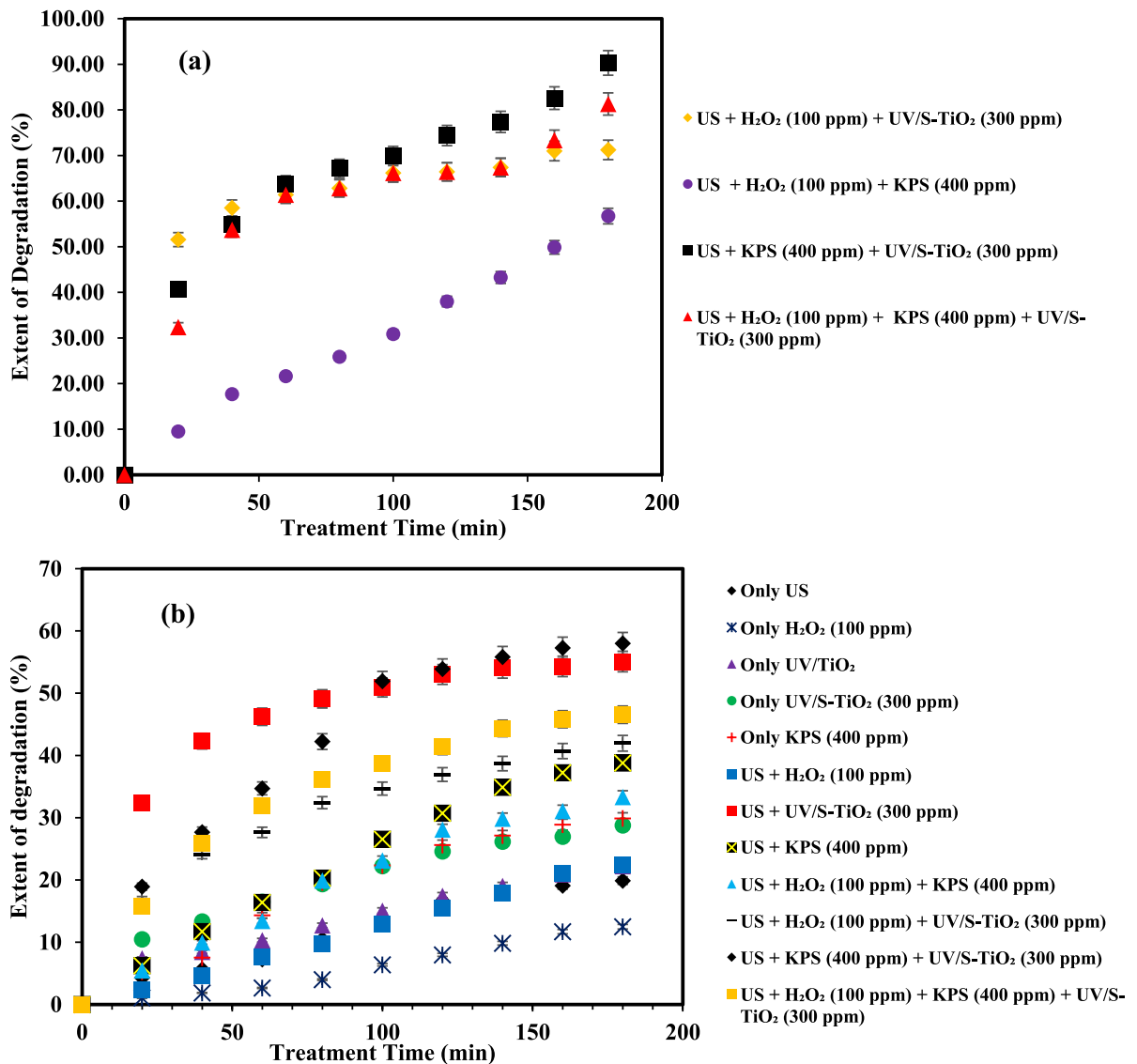


Fig. 12 a Decolourization behaviour of AR131 using combination approaches based on US, H₂O₂, KPS, and S-TiO₂ b Large-scale degradation of AR131 using various combination approaches

Bhosale (2013) studied different combinations involving HC (orifice), US, H₂O₂, sodium persulfate, and sodium hypochlorite (NaOCl) for the degradation of Orange Acid II. The best result was obtained using HC+NaOCl (8.08 × 10⁻⁵ mg/J as the cavitation yield). The selection of the best-performing intensifying agent is dependent on the nature of the pollutant, and the current study successfully established the best degradation approaches for the AR131 dye as US+KPS+UV/S-TiO₂ in terms of degradation extent and US+UV/S₂ in terms of synergy.

Scale-up studies

The optimum conditions of small-scale experiments have been scaled up to an operating capacity of 3 L using the US reactor to establish AR131 degradation at a pilot scale in the presence of H₂O₂, KPS, and UV/S-TiO₂. The degradation results for all the schemes have been presented in Fig. 12b. During the AR131 degradation using individual UV/S-TiO₂ (28.8%), UV/TiO₂ (22.22%), H₂O₂ (12.5%), and KPS (29.9%), the power dissipation while stirring was

kept similar to US assisted experiments. Based on the power consumption by the US, the rotation speed (rpm) of the overhead stirrer was determined based on the following equation:

$$P = N_p(\rho N^3 D^5) = \text{US rated power} \times \text{horn efficiency} \quad (8)$$

where N_p denotes the power number, ρ denotes the density of the AR131 solution, N denotes the stirring speed, and D denotes the diameter of the impeller. Taking N_p as 4.1 (for hollow blade turbine), ρ as 1000 kg/m^3 , D as 8 cm, US-rated power as 1000 W, and horn efficiency as 11.3%, the required speed of the overhead stirrer was obtained as approximately 1000 rpm.

When degradation of AR131 was carried out using the various combined approaches (without and with ultrasound), the degradation extent varied in the range between 12.5% and 58.01%. Table 1 shows the degradation results of the combined approaches at large scale. The inclusion of H_2O_2 was observed to be the least effective (12.5% and 22.49% degradation without and with ultrasound, respectively) because AR131 was quite resistant to the oxidation action of H_2O_2 . The higher resistance of chromophore to H_2O_2 oxidation compared to other oxidants was also reported by Guimarães et al. (2012) for the degradation of Reactive Black 19. They observed an insignificant effect on the dye concentration when H_2O_2

dosage was varied in the range of 100–800 mg/L. Frago et al. (2009) also observed that the degradation of Food Yellow 3 and Food Yellow 4 did not happen in the presence of only H_2O_2 .

It was observed that the large-scale application of US+KPS+UV/S- TiO_2 resulted in a maximum degradation of only 58.01%, which was less than the small-scale degradation as 90.3%. On a large scale, other than variation in the distribution of total output power per unit volume, a lack of control over temperature, also resulted in a somewhat lower extent of AR131 degradation. The intensity of ultrasonic cavitation decreases exponentially while moving away from the tip of the horn or the transducer, and hence it is important to decide on an optimum geometry. Type and number of transducers, temperature and pressure distribution, physicochemical properties, presence of solid particles or dissolved gases in a liquid, and erosion on reactor or pipe surfaces (Lévêque et al., 2018) are the factors to be properly analyzed to replicate the results on a larger scale equivalent to that of the small scale.

Sivakumar and Pandit (2001) studied the degradation of Rhodamine B, where they addressed the importance of power density and power intensity in deciding the degradation of a specific pollutant. It was reported that an optimum value of power exists because, due to the formation of larger bubble clouds at very high power, a decoupling effect takes place, thereby decreasing the degradation extent. The optimum parameter values vary depending on the type of ultrasonic equipment as the acoustic field varies. In their study, they considered power density to be more important than power intensity since that is associated with the total volume of the medium. A correlation between the percentage degradation of Rhodamine B and power density was reported in their work as follows:

$$\text{Degradation}(\%) = 75.883 \times \left(\frac{P}{V}\right)^{0.6418} \quad (9)$$

In our study, the small-scale operating power was 140 W with a horn efficiency of 8.2% and a medium volume of 200 mL. At a large scale, the rated power was 1000 W, with energy transfer efficiency of 11.3% and medium volume at 3 L. For both cases, the duty cycle was maintained at 70%. In the case of large scale, the individual US resulted in 19.89%

Table 1 Degradation efficacy for AR131 degradation using the large-scale US reactor approach

Large-Scale Treatment Scheme	Degradation Efficacy (%)
Only US	19.89
Only H_2O_2 (100 ppm)	12.5%
Only UV/ TiO_2 (300 ppm)	22.22
Only UV/S- TiO_2 (300 ppm)	28.8%
Only KPS (400 ppm)	28.9%
US + H_2O_2 (100 ppm)	22.49
US + KPS (400 ppm)	38.8
US + UV/S- TiO_2 (300 ppm)	55.1
US + H_2O_2 (100 ppm) + KPS (400 ppm)	33.33
US + H_2O_2 (100 ppm) + UV/S- TiO_2	41.96
US + KPS (400 ppm) + UV/S- TiO_2 (300 ppm)	58.01
US + H_2O_2 (100 ppm) + KPS (400 ppm) + UV/S- TiO_2 (300 ppm)	46.5

degradation, whereas, for small scale experimentation, the degradation was 36.31% for the individual US. Assuming the relationship between the percentage degradation of AR131 and power density as:

$$Degradation(\%) = A \times \left(\frac{P}{V}\right)^B \tag{10}$$

where, A and B are determined from the following two equations by substituting all values as:

$$36.31 = A \times \left(\frac{140 \times 0.7 \times 8.2}{200 \times 100}\right)^B \tag{11}$$

$$19.89 = A \times \left(\frac{1000 \times 0.7 \times 11.3}{3000 \times 100}\right)^B \tag{12}$$

Solving Eqs. (11 and 12), A was determined to be 2149.315 and B was determined to be 1.428. Thus, for the degradation of AR131, the correlation for predicting degradation was obtained by putting the values of A and B in Eq. (10) as:

$$Degradation(\%) = 2149.315 \times \left(\frac{P}{V}\right)^{1.428} \tag{13}$$

The correlation suggests that an adequate amount of energy must be provided for a particular degradation process to get the desired results, which can also assist in avoiding an oversupply of energy. Although this correlation cannot be used as a generalized one since, for each type of device an optimum power density should exist, beyond which the degradation does not increase with a further rise in the power density. The correlation is also dependent on the type of pollutant. It is important to note that the developed correlation suggests the approach to be followed for analyzing the impact of the power density on degradation.

The quantification of the chemical activity is portrayed by the cavitation yield, which is typically used for the quantification of the cavitation effects. Cavitation yield is defined as the amount of pollutant degraded (mg) per unit of energy supplied (J) (Patil et al., 2021a, b). The determined values of cavitation yield have been shown in Table 2 whereas the method of calculation has been represented in Appendix A and B. In the current study for the small-scale operation, the maximum cavitation yield was obtained for US+KPS (400 ppm)+UV/S-TiO₂ (300 ppm, 2:1) with a value of 8.96×10⁻⁶ mg/J and a degradation extent of 90.29%.

Hence, the cavitation yield is greater for approaches with a higher extent of AR131 degradation. The cavitation yield obtained for the approaches of US+H₂O₂ (100 ppm), US+KPS (400 ppm), US+UV/S-TiO₂ (300 ppm, 2:1), US+H₂O₂ (100 ppm)+UV/S-TiO₂ (300 ppm, 2:1), and US+H₂O₂ (100 ppm)+KPS (400 ppm)+UV/S-TiO₂ (300 ppm, 2:1) was 1.90×10⁻⁶, 3.24×10⁻⁶, 4.11×10⁻⁶, 7.07×10⁻⁶, and 8.06×10⁻⁶ mg/J, respectively. Similarly, the maximum cavitation yield for the large-scale study was obtained for the approach of US+KPS (400 ppm)+UV/S-TiO₂ (300 ppm, 2:1) with a value of 5.75×10⁻⁶ mg/J at the optimum loadings of the oxidants and catalyst. The cavitation yield obtained for US+H₂O₂ (100 ppm), US+KPS (400 ppm), US+UV/S-TiO₂ (300 ppm, 2:1), US+H₂O₂ (100 ppm)+UV/S-TiO₂ (300 ppm, 2:1), and US+H₂O₂ (100 ppm)+KPS (400 ppm)+UV/S-TiO₂ (300 ppm, 2:1) was 2.23×10⁻⁶, 3.85×10⁻⁶, 5.47×10⁻⁶, 4.16×10⁻⁶, and 4.62×10⁻⁶ mg/J, respectively. The cavitation yield was higher at the large scale compared to the small scale, which was attributed to the higher energy efficacy of the US reactor compared to the US horn. Although, the exception of US+KPS (400 ppm)+UV/S-TiO₂ (300 ppm, 2:1), US+H₂O₂ (100 ppm)+UV/S-TiO₂ (300 ppm, 2:1), and US+H₂O₂ (100 ppm)+KPS (400 ppm)+UV/S-TiO₂ (300 ppm, 2:1) were observed with higher cavitation yield for small scale compared to large scale which was attributed to the higher extent of AR131 degradation for US horn compared to the US reactor for these approaches. Therefore, the large-scale US reactor can be a quite economical option compared to the small-scale US horn for the similar extent of AR131 degradation. In addition, the economic feasibility of the US reactor increases with the increase in the extent of degradation, and therefore a higher degradation amount is prerequisite to improve the economic feasibility.

The rate constants for the various approaches on a large scale were determined by plotting -ln(C/C₀) vs. treatment time, and the corresponding rate constants were utilized for the determination of synergistic coefficients, which have been presented in Table 3. Interestingly, the combination of US with UV/S-TiO₂ resulted in the highest synergistic coefficient of 1.61, similar to what was observed in small-scale batches. Thus, this scheme can be considered to obtain maximum efficacy in terms of synergy in degrading AR131.

Table 2 Cavitation yield for the various oxidation approaches

Oxidation Approach	AR131 Degradation (%)	AR131 Degradation (mg/L)	Cavitation Yield (mg/J)
US Horn (25 ppm, pH 4, 100 W)	16.64	4.16	7.86×10^{-7}
US Horn (25 ppm, pH 6, 100 W)	13.53	3.3825	6.39×10^{-7}
US Horn (25 ppm, pH 11.7, 100 W)	6.83	1.7075	3.23×10^{-7}
US Horn (80 W, pH 3)	19.31	4.83	9.12×10^{-7}
US Horn (100 W, pH 3)	20.41	5.10	9.64×10^{-7}
US Horn (120 W, pH 3)	28.17	7.04	1.33×10^{-6}
US Horn (130 W, pH 3)	30.34	7.58	1.43×10^{-6}
US Horn (140 W, pH 3) {Optimized}	36.31	9.08	1.72×10^{-6}
US Horn/H ₂ O ₂ (50 ppm)	37.38	9.34	1.77×10^{-6}
US Horn/H ₂ O ₂ (100 ppm)	40.14	10.03	1.90×10^{-6}
US Horn/H ₂ O ₂ (500 ppm)	23.91	5.98	1.13×10^{-6}
US Horn/UV/S-TiO ₂ (300 ppm, 1:1)	39.11	9.78	1.85×10^{-6}
US Horn/UV/S-TiO ₂ (300 ppm, 2:1)	86.96	21.74	4.11×10^{-6}
US Horn/UV/S-TiO ₂ (300 ppm, 3:1)	52.00	13.00	2.46×10^{-6}
US Horn/KPS (100 ppm)	44.04	11.01	2.08×10^{-6}
US Horn/KPS (200 ppm)	48.99	12.25	2.31×10^{-6}
US Horn/KPS (300 ppm)	53.23	13.31	2.51×10^{-6}
US Horn/KPS (400 ppm)	68.58	17.14	3.24×10^{-6}
US Horn/H ₂ O ₂ /KPS (100 ppm H ₂ O ₂ , 400 ppm KPS)	56.73	14.18	2.68×10^{-6}
US Horn/H ₂ O ₂ /UV/S-TiO ₂ (100 ppm H ₂ O ₂ , 300 ppm S-TiO ₂ (2:1))	71.23	17.81	7.07×10^{-6}
US Horn/KPS/UV/S-TiO ₂ (400 ppm KPS, 300 ppm S-TiO ₂ (2:1))	90.29	22.57	8.96×10^{-6}
US Horn/H ₂ O ₂ /KPS/UV/S-TiO ₂ (100 ppm H ₂ O ₂ , 400 ppm KPS, 300 ppm S-TiO ₂ (2:1))	81.29	20.32	8.06×10^{-6}
US Reactor/H ₂ O ₂ (100 ppm H ₂ O ₂ , 1000 W)	22.49	5.62	2.23×10^{-6}
US Reactor/KPS (400 ppm KPS, 1000 W)	38.80	9.70	3.85×10^{-6}
US Reactor/UV/S-TiO ₂ (300 ppm S-TiO ₂ (2:1), 1000 W)	55.09	13.77	5.47×10^{-6}
US Reactor/H ₂ O ₂ /KPS (100 ppm H ₂ O ₂ , 400 ppm KPS, 1000 W)	33.33	8.33	3.31×10^{-6}
US Reactor/H ₂ O ₂ /UV/S-TiO ₂ (100 ppm H ₂ O ₂ , 300 ppm S-TiO ₂ (2:1), 1000 W)	41.96	10.49	4.16×10^{-6}
US Reactor/KPS/UV/S-TiO ₂ (400 ppm KPS, 300 ppm S-TiO ₂ (2:1), 1000 W)	58.01	14.50	5.75×10^{-6}
US Reactor/H ₂ O ₂ /KPS/UV/S-TiO ₂ (100 ppm H ₂ O ₂ , 400 ppm KPS, 300 ppm S-TiO ₂ (2:1), 1000 W)	46.55	11.64	4.62×10^{-6}

In some of the combination approaches, the overall kinetic rate constant did not show any improvement compared to the sum of the rate constants for the individual approaches. Hence, these hybrid techniques may show lesser efficiency due to the parallel reactions taking place in the reactor which produce radicals having less oxidation potential than the $\bullet\text{OH}$ and $\text{SO}_4^{\bullet-}$ radicals. Due to these undesirable side reactions and radical scavenging actions, the synergetic coefficient comes out to be lower. Hence, the investigation of the combined oxidation approaches is a prerequisite for determining the most effective approach,

Table 3 Synergetic coefficients for different combination schemes at large scale

Treatment Scheme	Synergetic Coefficient
US + H ₂ O ₂	0.6667
US + KPS	0.8056
US + UV/S-TiO ₂	1.6111
US + H ₂ O ₂ + KPS	0.5814
US + H ₂ O ₂ + UV/S-TiO ₂	0.8372
US + KPS + UV/S-TiO ₂	1
US + H ₂ O ₂ + KPS + UV/S-TiO ₂	0.6462

as in some cases the degradation extent may not be synergistic due to undesirable side reactions. In addition, the AR131 degradation extent in the case of the large scale US reactor was quite less than that for the small scale US horn. The combined approach of US + KPS + UV/S-TiO₂ with 90.29% degradation was the most efficient at lab scale, however, the large scale approach of US + KPS + UV/S-TiO₂ resulted in only 58.01% degradation. The scale up study using the single horn US reactor suggested that a more efficient US reactor can be used for US irradiation instead of the single horn US reactor, which provided US irradiation insufficient to degrade the recalcitrant AR131 dye. Therefore, in the future, the utilization of a dual frequency US reactor with multiple transducers attached to the walls can be used for the scale up study. The higher amount of US irradiation typically increases the quantum of the cavitation events and therefore reduces the loadings of the various chemical oxidants required to enhance the generation of •OH radicals. Lower the utilization of chemical oxidants, the higher would be environmental viability of the methods utilized for degradation. Hence, the implementation of US reactors combined with the hybrid AOPs increases the environmental friendliness of the degradation process. Overall, the study clearly confirms that it is important to select the best combination for the specific pollutant in question as per the methodology presented in the current work.

Conclusions

Ultrasound can be considered one of the efficient techniques that can provide higher efficiency in the degradation of various pollutants at modest power consumption and low operating costs, under optimized operation. In the current study, US-based degradation of AR131 has shown promising results at small as well as large scales of operation. In the case of AR131, an acidic pH of 3, an optimum initial concentration as 25 mg/L, and an optimum input power of 140 W resulted in the highest extent of degradation using the individual approach. In the combined approach of US + H₂O₂, the degradation first increased and then decreased with the increase of H₂O₂ dosage, whereas for the US + KPS approach, the degradation extent increased monotonously

with the increase in KPS dosage. It was thus concluded that AR131 showed resistance to the oxidizing property of H₂O₂. The approach of US + H₂O₂ (100 ppm) achieved a marginal increase in the degradation extent to that obtained with individual US. The use of KPS and UV/S-TiO₂ intensified the degradation by a considerable amount (68.54% and 86.97% as degradation, respectively, compared to only 36.31% for only US at a small scale). With the inclusion of two or three additives simultaneously, the degradation extent decreases due to the excessive presence of free radicals and the consequent shift of the reaction equilibrium towards the recombination reactions. For example, the US + H₂O₂ + KPS approach resulted in lower degradation (56.73%) compared to the US + KPS (68.54%) approach. Similarly, the US + H₂O₂ + KPS + UV/S-TiO₂ approach resulted in lower degradation (81.29%) compared to the US + UV/S-TiO₂ (86.97%) and US + KPS + UV/S-TiO₂ (90.3%) approaches. Thus, it is important to select the right combination for the specific dye in question, confirming the importance of the current work that elucidates effect for AR131 for the first time. A relationship between power density and degradation extent was successfully established, taking into account the observations from the small and large-scale experiments. The maximum degradation was achieved for the approach of US + KPS + UV/S-TiO₂ for both small (90.3%) and large scale (58.01%) studies. However, the synergistic coefficient for the approach of US + KPS + UV/S-TiO₂ (1.07 and 1 for small and large scales respectively) was lesser compared to the US + UV/S-TiO₂ (1.61 and 1.57 for small and large scale respectively). Therefore, the approach of US + KPS + UV/S-TiO₂ was the most efficient in terms of the extent of degradation achieved, whereas the approach of US + UV/S-TiO₂ was the most efficient in terms of synergy at small and large scales, respectively.

Authors' contributions Subhamita Das: Experimental methodology, Investigation, Writing the first draft. Chandrodai Agarkoti: Data Analysis, Review and Editing of draft. Parag R. Gogate: Supervision, Reviewed and Editing of draft.

Funding CA would like to acknowledge the funding from DST as a fellowship during the PhD degree. SD would like to acknowledge the funding of AICTE for fellowship during the Master's degree.

Data availability Data will be made available on request.

Declarations

Ethical approval All authors have read, understood, and have complied as applicable with the statement on "Ethical responsibilities of Authors" as found in the Instructions for Authors and are aware that with minor exceptions, no changes can be made to authorship once the paper is submitted.

Competing interests The authors declare no competing interests.

Appendix A: Cavitation yield for the AR131 degradation using US horn

Volume = 200 mL

Time = 180 min

Optimum input power = 140 W

Duty cycle = 70%

Power dissipation per unit volume = 700 W/L

Energy dissipation per unit volume = (Power dissipation per unit volume \times Time \times Duty cycle) / 100 = 5,292,000 J/L

AR131 degraded in 180 min for US+KPS+UV/S-TiO₂ = (AR131 degradation (%) \times Initial concentration) / 100 = (90.29 \times 25) / 100 = 22.57 mg/L

Cavitation yield = AR131 degraded in 180 min / Energy dissipation per unit volume = 8.96 \times 10⁻⁶ mg/J

Appendix B: Cavitation yield for the AR131 degradation using US reactor

Volume = 3000 mL

Time = 180 min

Optimum input power = 1000 W

Duty cycle = 70%

Power dissipation per unit volume = 333.33 W/L

Energy dissipation per unit volume = (Power dissipation per unit volume \times Time \times Duty cycle) / 100 = 2,520,000 J/L

AR131 degraded in 180 min for US+KPS+UV/S-TiO₂ = (AR131 degradation (%) \times Initial concentration) / 100 = (58.01 \times 25) / 100 = 14.50 mg/L

Cavitation yield = AR131 degraded in 180 min / Energy dissipation per unit volume = 5.75 \times 10⁻⁶ mg/J

References

- Agarkoti, C., Chaturvedi, A., Gogate, P. R., & Pandit, A. B. (2023). Degradation of sulfamerazine using ultrasonic horn and pilot scale US reactor in combination with different oxidation approaches. *Separation and Purification Technology*, 312, 123351.
- Agarkoti, C., Gogate, P. R., & Pandit, A. B. (2022). Coupling of acoustic/hydrodynamic cavitation with ozone (O₃), hydrogen peroxide (H₂O₂), magnesium oxide (MgO) and manganese dioxide (MnO₂) for the effective treatment of CETP effluent. *Separation and Purification Technology*, 284, 120281.
- Agarkoti, C., Thanekar, P., & Gogate, P. (2021). Cavitation based treatment of industrial wastewater: A critical review focusing on mechanisms, design aspects, operating conditions and application to real effluents. *Journal of Environmental Management*, 300, 113786.
- Akhter, P., Arshad, A., Saleem, A., & Hussain, M. (2022). Recent development in non-metal-doped titanium dioxide photocatalysts for different dyes degradation and the study of their strategic factors: A review. *Catalysts*, 12(11), 1331.
- Alkaykh, S., Mbarek, A., & Ali-Shattle, E. E. (2020). Photocatalytic degradation of methylene blue dye in aqueous solution by MnTiO₃ nanoparticles under sunlight irradiation. *Heliyon*, 6(4), e03663.
- Almomani, F. A., Shawaqfeh, M., Bhosale, R. R., & Kumar, A. (2016). Removal of emerging pharmaceuticals from wastewater by ozone-based advanced oxidation processes. *Environmental Progress & Sustainable Energy*, 35(4), 982–995.
- Batra, V., Kaur, I., Pathania, D., & Chaudhary, V. (2022). Efficient dye degradation strategies using green synthesized ZnO-based nanoplateforms: A review. *Applied Surface Science Advances*, 11, 100314.
- Benomara, A., Guenfoud, F., Mokhtari, M., & Boudjemaa, A. (2021). Sonolytic, sonocatalytic and sonophotocatalytic degradation of a methyl violet 2B using iron-based catalyst. *Reaction Kinetics, Mechanisms and Catalysis*, 132, 513–528.
- Bera, S. P., & Tank, S. (2021). Microbial degradation of Procion Red by *Pseudomonas stutzeri*. *Scientific Reports*, 11(1), 1–12.
- Böbl, F., Menzel, V. C., Chatzisyneon, E., Comyn, T. P., Cowin, P., Cobley, A. J., & Tudela, I. (2023). Effect of frequency and power on the piezocatalytic and sonochemical degradation of dyes in water. *Chemical Engineering Journal Advances*, 14, 100477.
- Çalışkan, Y., Yatmaz, H. C., & Bektaş, N. (2017). Photocatalytic oxidation of high concentrated dye solutions enhanced by hydrodynamic cavitation in a pilot reactor. *Process Safety and Environmental Protection*, 111, 428–438.
- Daware, G., & Gogate, P. (2021). Intensified sonochemical degradation of 2-Picoline in combination with advanced oxidizing agents. *Ultrasonics Sonochemistry*, 77, 105702.
- Dhanke, P. B., & Wagh, S. M. (2020). Intensification of the degradation of Acid RED-18 using hydrodynamic cavitation. *Emerging Contaminants*, 6, 20–32.
- Duan, B., Zhu, Z., Sun, C., Zhou, J., & Walsh, A. (2020). Preparing copper catalyst by ultrasound-assisted chemical precipitation method. *Ultrasonics Sonochemistry*, 64, 105013.
- Dükkancı, M., & Gündüz, G. (2006). Ultrasonic degradation of oxalic acid in aqueous solutions. *Ultrasonics Sonochemistry*, 13(6), 517–522.

- Fedorov, K., Dinesh, K., Sun, X., Soltani, R. D. C., Wang, Z., Sonawane, S., & Boczkaj, G. (2022). Synergistic effects of hybrid advanced oxidation processes (AOPs) based on hydrodynamic cavitation phenomenon—a review. *Chemical Engineering Journal*, 432, 134191.
- Fragoso, C. T., Battisti, R., Miranda, C., & de Jesus, P. C. (2009). Kinetic of the degradation of CI Food Yellow 3 and CI Food Yellow 4 azo dyes by the oxidation with hydrogen peroxide. *Journal of Molecular Catalysis a: Chemical*, 301(1–2), 93–97.
- Gaya, U. I., & Abdullah, A. H. (2008). Heterogeneous photocatalytic degradation of organic contaminants over titanium dioxide: A review of fundamentals, progress and problems. *Journal of Photochemistry and Photobiology c: Photochemistry Reviews*, 9(1), 1–12.
- Ghumra, D. P., Agarkoti, C., & Gogate, P. R. (2021). Improvements in effluent treatment technologies in Common Effluent Treatment Plants (CETPs): Review and recent advances. *Process Safety and Environmental Protection*, 147, 1018–1051.
- Goel, M., Hongqiang, H., Mujumdar, A. S., & Ray, M. B. (2004). Sonochemical decomposition of volatile and non-volatile organic compounds—a comparative study. *Water Research*, 38(19), 4247–4261.
- Gogate, P. R. (2022). Intensified sulfate radical oxidation using cavitation applied for wastewater treatment. *Current Opinion in Chemical Engineering*, 37, 100850.
- Gogate, P. R., & Bhosale, G. S. (2013). Comparison of effectiveness of acoustic and hydrodynamic cavitation in combined treatment schemes for degradation of dye wastewaters. *Chemical Engineering and Processing: Process Intensification*, 71, 59–69.
- Gore, M. M., Saharan, V. K., Pinjari, D. V., Chavan, P. V., & Pandit, A. B. (2014). Degradation of reactive orange 4 dye using hydrodynamic cavitation based hybrid techniques. *Ultrasonics Sonochemistry*, 21(3), 1075–1082.
- Guimarães, J. R., Maniero, M. G., & de Araújo, R. N. (2012). A comparative study on the degradation of RB-19 dye in an aqueous medium by advanced oxidation processes. *Journal of Environmental Management*, 110, 33–39.
- Hussain, S. T., Mazhar, M., Siddiq, A., Javid, H., & Siddiq, M. (2012). Cu-S coped TiO₂ nanophotocatalyst for the degradation of environmental and industrial pollutants. *The Open Catalysis Journal*, 5, 21–30.
- Humayun, M., Raziq, F., Khan, A., & Luo, W. (2018). Modification strategies of TiO₂ for potential applications in photocatalysis: A critical review. *Green Chemistry Letters and Reviews*, 11(2), 86–102.
- Ibhadon, A. O., & Fitzpatrick, P. (2013). Heterogeneous photocatalysis: Recent advances and applications. *Catalysts*, 3(1), 189–218.
- Kamal, I. M., Abdeltawab, N. F., Ragab, Y. M., Farag, M. A., & Ramadan, M. A. (2022). Biodegradation, decolorization, and detoxification of di-azo dye direct Red 81 by halotolerant, alkali-thermo-tolerant bacterial mixed cultures. *Microorganisms*, 10(5), 994.
- Karami, M., Sharafi, K., Asadi, A., Bagheri, A., Yosefvand, F., Charganeh, S. S., Mirzaei, N., & Velayati, A. (2016). Degradation of Reactive Red 198 (RR198) from aqueous solutions by advanced oxidation processes (AOPs): O₃, H₂O₂/O₃ and H₂O₂/ultrasonic. *Bulgarian Chemical Communications*, 48(Special), 43–49.
- Karpuraranjith, M., Chen, Y., Rajaboopathi, S., Ramadoss, M., Srinivas, K., Yang, D., & Wang, B. (2022). Three-dimensional porous MoS₂ nanobox embedded g-C₃N₄@ TiO₂ architecture for highly efficient photocatalytic degradation of organic pollutant. *Journal of Colloid and Interface Science*, 605, 613–623.
- Khan, S., Han, C., Khan, H. M., Boccelli, D. L., Nadagouda, M. N., & Dionysiou, D. D. (2017). Efficient degradation of lindane by visible and simulated solar light-assisted S-TiO₂/peroxymonosulfate process: Kinetics and mechanistic investigations. *Molecular Catalysis*, 428, 9–16.
- Khandegar, V., & Saroha, A. K. (2014). Electrochemical treatment of textile effluent containing Acid Red 131 dye. *Journal of Hazardous, Toxic, and Radioactive Waste*, 18(1), 38–44.
- Kongor, A., Panchal, M., Athar, M., Vora, M., Makwana, B., Jha, P., & Jain, V. (2021). Calix [4] pyrrole stabilized PdNPs as an efficient heterogeneous catalyst for enhanced degradation of water-soluble carcinogenic Azo dyes. *Catalysis Letters*, 151, 548–558.
- Kumar, M. S., Sonawane, S., Bhanvase, B., & Bethi, B. (2018). Treatment of ternary dye wastewater by hydrodynamic cavitation combined with other advanced oxidation processes (AOP's). *Journal of Water Process Engineering*, 23, 250–256.
- Kumar, M. S., Sonawane, S., & Pandit, A. B. (2017). Degradation of methylene blue dye in aqueous solution using hydrodynamic cavitation based hybrid advanced oxidation processes. *Chemical Engineering and Processing: Process Intensification*, 122, 288–295.
- Lakshmi, N., Gogate, P. R., & Pandit, A. B. (2021). Treatment of acid violet 7 dye containing effluent using the hybrid approach based on hydrodynamic cavitation. *Process Safety and Environmental Protection*, 153, 178–191.
- Lévêque, J.-M., Cravotto, G., Delattre, F., & Cintas, P. (2018). Scaling-up enabling the full potential of industrial applications of ultrasound and hydrodynamic cavitation. In *Organic Sonochemistry: Challenges and Perspectives for the 21st Century*. Ed. Lévêque, J.-M., Cravotto, G., Delattre, F., Cintas, P. (pp. 113–123). Springer.
- Mahendran, V., & Gogate, P. R. (2021). Degradation of Acid Scarlet 3R dye using oxidation strategies involving photocatalysis based on Fe doped TiO₂ photocatalyst, ultrasound and hydrogen peroxide. *Separation and Purification Technology*, 274, 119011.
- Manousaki, E., Psillakis, E., Kalogerakis, N., & Mantzavinos, D. (2004). Degradation of sodium dodecylbenzene sulfonate in water by ultrasonic irradiation. *Water Research*, 38(17), 3751–3759.
- More, N. S., & Gogate, P. R. (2018). Intensification of degumming of crude soybean oil using ultrasound in combination with oxidizing agents. *Chemical Engineering and Processing-Process Intensification*, 128, 132–142.
- Mosleh, S., Rahimi, M., Ghaedi, M., & Dashtian, K. (2016). Sonophotocatalytic degradation of trypan blue and vesuvine dyes in the presence of blue light active photocatalyst of Ag₃PO₄/Bi₂S₃-HKUST-1-MOF: Central composite optimization and synergistic effect study. *Ultrasonics Sonochemistry*, 32, 387–397.
- Nam, S.-H., Kim, T. K., & Boo, J.-H. (2012). Physical property and photo-catalytic activity of sulfur doped TiO₂

- catalysts responding to visible light. *Catalysis Today*, 185(1), 259–262.
- Nayebi, B., Ghalebizade, M., & Niyavol, K. P. (2021). Removal of Acid Red 131 by peroxi-coagulation using stainless steel and aluminum electrodes: A comparative study. *Water Conservation Science and Engineering*, 6(4), 201–211.
- Patil, N. N., & Shukla, S. R. (2015). Degradation of Reactive Yellow 145 dye by persulfate using microwave and conventional heating. *Journal of Water Process Engineering*, 7, 314–327.
- Patil, P., Raut-Jadhav, S., & Pandit, A. (2021a). Effect of intensifying additives on the degradation of thiamethoxam using ultrasound cavitation. *Ultrasonics Sonochemistry*, 70, 105310.
- Patil, P. B., Bhandari, V. M., & Ranade, V. V. (2021b). Wastewater treatment and process intensification for degradation of solvents using hydrodynamic cavitation. *Chemical Engineering and Processing-Process Intensification*, 166, 108485.
- Piątkowska, A., Janus, M., Szymański, K., & Mozia, S. (2021). C-, N- and S-doped TiO₂ photocatalysts: A review. *Catalysts*, 11(1), 144.
- Prabakaran, E., & Pillay, K. (2019). Synthesis of N-doped ZnO nanoparticles with cabbage morphology as a catalyst for the efficient photocatalytic degradation of methylene blue under UV and visible light. *RSC Advances*, 9(13), 7509–7535.
- Rajashekarappa, K. K., Mahadevan, G. D., Neelagund, S. E., Sathynarayana, M., Vijaya, D., & Mulla, S. I. (2022). Decolorization of amaranth RI and fast red E azo dyes by thermophilic *Geobacillus thermoleovorans* KNG 112. *Journal of Chemical Technology & Biotechnology*, 97(2), 482–489.
- Rajoriya, S., Bargole, S., & Saharan, V. K. (2017). Degradation of reactive blue 13 using hydrodynamic cavitation: Effect of geometrical parameters and different oxidizing additives. *Ultrasonics Sonochemistry*, 37, 192–202.
- Rajoriya, S., Carpenter, J., Saharan, V. K., & Pandit, A. B. (2016). Hydrodynamic cavitation: An advanced oxidation process for the degradation of bio-refractory pollutants. *Reviews in Chemical Engineering*, 32(4), 379–411.
- Raut-Jadhav, S., Pinjari, D. V., Saini, D. R., Sonawane, S. H., & Pandit, A. B. (2016). Intensification of degradation of methomyl (carbamate group pesticide) by using the combination of ultrasonic cavitation and process intensifying additives. *Ultrasonics Sonochemistry*, 31, 135–142.
- Reza, K. M., Kurny, A., & Gulshan, F. (2017). Parameters affecting the photocatalytic degradation of dyes using TiO₂: A review. *Applied Water Science*, 7(4), 1569–1578.
- Saharan, V. K., Badve, M. P., & Pandit, A. B. (2011). Degradation of Reactive Red 120 dye using hydrodynamic cavitation. *Chemical Engineering Journal*, 178, 100–107.
- Sivakumar, M., & Pandit, A. B. (2001). Ultrasound enhanced degradation of Rhodamine B: Optimization with power density. *Ultrasonics Sonochemistry*, 8(3), 233–240.
- Slama, H. B., Chenari Bouket, A., Pourhassan, Z., Alenezi, F. N., Silini, A., Cherif-Silini, H., Oszako, T., Luptakova, L., Golińska, P., & Belbahri, L. (2021). Diversity of synthetic dyes from textile industries, discharge impacts and treatment methods. *Applied Sciences*, 11(14), 6255.
- Soumia, F., & Petrier, C. (2016). Effect of potassium monopersulfate (oxone) and operating parameters on sonochemical degradation of cationic dye in an aqueous solution. *Ultrasonics Sonochemistry*, 32, 343–347.
- Thamaphat, K., Limsuwan, P., & Ngotawornchai, B. (2008). Phase characterization of TiO₂ powder by XRD and TEM. *Agriculture and Natural Resources*, 42(5), 357–361.
- Thanekar, P., & Gogate, P. R. (2019). Combined hydrodynamic cavitation based processes as an efficient treatment option for real industrial effluent. *Ultrasonics Sonochemistry*, 53, 202–213.
- Umebayashi, T., Yamaki, T., Itoh, H., & Asai, K. (2002). Band gap narrowing of titanium dioxide by sulfur doping. *Applied Physics Letters*, 81(3), 454–456.
- Vončina, D. B., & Majcen-Le-Marechal, A. (2003). Reactive dye decolorization using combined ultrasound/H₂O₂. *Dyes and Pigments*, 59(2), 173–179.
- Wang, K., Jin, R.-Y., Qiao, Y.-N., He, Z.-D., Wang, Y., & Wang, X.-J. (2019). The removal of Rhodamine B by H₂O₂ or ClO₂ combined with hydrodynamic cavitation. *Water Science and Technology*, 80(8), 1571–1580.
- Wang, X., Jia, J., & Wang, Y. (2011). Degradation of CI Reactive Red 2 through photocatalysis coupled with water jet cavitation. *Journal of Hazardous Materials*, 185(1), 315–321.
- Watzke, E., & Kloss, T. (1996). Borosilicate glass having improved UV transmission, thermal and chemical properties and methods of making and using same. United States patent 5,547,904. Aug 20, 1996.
- Wijetunga, S., Xiufen, L., Wenquan, R., & Chen, J. (2012). Removal mechanisms of acid dyes of different chemical groups under anaerobic mixed culture. *Ruhuna Journal of Science*, 2(1), 96–110.
- Wu, C.-H. (2007). Sonocatalytic degradation of CI Reactive Red 198 in H₂O₂-based systems. *Reaction Kinetics and Catalysis Letters*, 92(2), 377–384.
- Xie, A., Zhou, X., Zhou, W., Luo, S., & Yao, C. (2017). Preparation and enhanced photocatalytic activity of S-doped TiO₂/palygorskite composites. *Materials Technology*, 32(4), 265–271.
- Yaseen, D., & Scholz, M. (2019). Textile dye wastewater characteristics and constituents of synthetic effluents: A critical review. *International Journal of Environmental Science and Technology*, 16(2), 1193–1226.
- Zafar, Z., Fatima, R., & Kim, J.-O. (2021). Experimental studies on water matrix and influence of textile effluents on photocatalytic degradation of organic wastewater using Fe-TiO₂ nanotubes: Towards commercial application. *Environmental Research*, 197, 111120.
- Zampeta, C., Bertaki, K., Triantaphyllidou, I.-E., Frontistis, Z., & Vayenas, D. V. (2021). Treatment of real industrial-grade dye solutions and printing ink wastewater using a novel pilot-scale hydrodynamic cavitation reactor. *Journal of Environmental Management*, 297, 113301.

Publisher's Note Springer Nature remains neutral with regard to jurisdictional claims in published maps and institutional affiliations.

Springer Nature or its licensor (e.g. a society or other partner) holds exclusive rights to this article under a publishing agreement with the author(s) or other rightsholder(s); author self-archiving of the accepted manuscript version of this article is solely governed by the terms of such publishing agreement and applicable law.